



RADIOMETRIC ANALYSIS OF DAYTIME SATELLITE DETECTION

THESIS

Katherine B. Lilevjen, 2nd Lieutenant, USAF

AFIT/GAP/ENP/06-09

**DEPARTMENT OF THE AIR FORCE
AIR UNIVERSITY**

AIR FORCE INSTITUTE OF TECHNOLOGY

Wright-Patterson Air Force Base, Ohio

APPROVED FOR PUBLIC RELEASE; DISTRIBUTION UNLIMITED

The views expressed in this thesis are those of the author and do not reflect the official policy or position of the United States Air Force, Department of Defense, or the United States Government.

AFIT/GAP/ENP/06-09

RADIOMETRIC ANALYSIS OF DAYTIME SATELLITE DETECTION

THESIS

Presented to the Faculty

Department of Engineering Physics

Graduate School of Engineering and Management

Air Force Institute of Technology

Air University

Air Education and Training Command

In Partial Fulfillment of the Requirements for the

Degree of Master of Science (Applied Physics)

Katherine B. Lilevjen, BS

2nd Lieutenant, USAF

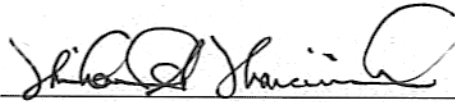
March 2006

APPROVED FOR PUBLIC RELEASE; DISTRIBUTION UNLIMITED.

RADIOMETRIC ANALYSIS OF DAYTIME SATELLITE DETECTION

Katherine B. Lilevjen, BS
2nd Lieutenant, USAF

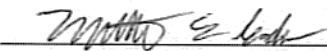
Approved:



Michael A. Marciniak (Chairman)

3 Mar 06

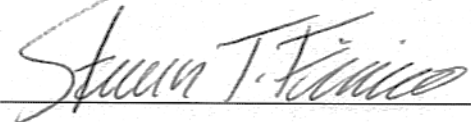
date



Matthew E. Goda (Member)

10 MAR 06

date



Steven T. Fiorino (Member)

10 MAR 06

date

Abstract

A radiometric model for daylight satellite detection is developed and used to evaluate the effects of various parameters on signal-to-noise ratio (SNR). Detection of reflected sunlight from a low-earth orbit, diffuse, planar satellite by a single-pixel infrared photovoltaic detector is considered. Noise considered includes photon noise from the background and signal, as well as thermal noise. Parameters considered include atmospheric conditions, optical parameters, and detector parameters. The Phillips Laboratory Expert-assisted User System, an atmospheric modeling tool that employs the MODTRAN and FASCODE transmission codes, is used to model wavelength-dependent atmospheric transmission and background radiance.

The SNR is found to increase when the detector is placed at higher altitudes and when there is lower aerosol content in the atmosphere. The SNR is also found to increase with decreased noise-equivalent bandwidth, detector dark current and field of view (FOV), and with larger optical elements. For a 16" diameter telescope and a FOV no smaller than 70 mrad, optimal bands are found to be between 0.8 μm and 1.7 μm .

Acknowledgements

I would like to thank my faculty advisor, Dr. Michael Marciniak, for his insight, explanations, and guidance throughout the thesis process. I would also like to thank my committee members, Lt Col Matthew Goda and Lt Col Steven Fiorino, for their interest and assistance. Finally, I would like to thank my husband for his patience and support.

Katherine B. Lilevjen

Table of Contents

| | Page |
|--|------|
| Acknowledgements | v |
| List of Figures | viii |
| List of Tables..... | x |
| I. Introduction..... | 1 |
| Literature Review | 2 |
| Problem Statement..... | 4 |
| Research Approach..... | 5 |
| Organization | 5 |
| II. Radiometry and Detection Background..... | 7 |
| Radiometric process | 7 |
| Terms and Units | 7 |
| Signal-to-Noise Ratio | 13 |
| Summary | 19 |
| III. Modeling | 20 |
| Signal Irradiance..... | 20 |
| Other parameters affecting the signal..... | 24 |
| Transmission of atmosphere..... | 25 |
| Transmission of optics..... | 25 |
| Transmission of filters..... | 26 |
| Quantum efficiency | 26 |
| Wavelength and Wavenumber..... | 28 |
| Background radiance | 30 |
| Field of View..... | 30 |
| Optics | 31 |
| Reflectance of the Satellite..... | 31 |
| Solar Radiance..... | 32 |
| Angular extent of satellite..... | 34 |
| Noise-equivalent Bandwidth | 34 |
| Detector Parameters..... | 35 |
| Variables with units and default values | 37 |
| PLEXUS-determined atmospheric transmission and background radiation..... | 39 |
| Approximations..... | 40 |
| Parameters investigated in this research | 44 |
| IV. Analysis and Results | 45 |
| Validation | 46 |
| Optimal bands..... | 48 |
| Field of View Survey..... | 52 |
| Detector Survey..... | 54 |
| Thermal Emissions | 54 |

| | |
|---|----|
| Visibility Survey..... | 56 |
| Aerosol Survey..... | 59 |
| Altitude Survey..... | 60 |
| Observation Angle Survey | 61 |
| Limits on Angular Extent of the Satellite | 64 |
| Summary | 65 |
| V. Conclusions | 67 |
| Using the Model to Analyze and Optimize Detection Systems..... | 67 |
| Recommendations for Future Research..... | 69 |
| Appendix A. <i>Mathematica</i> Code for Daytime Satellite Detection Model | 73 |
| Appendix B. <i>Mathematica</i> Code for Determining Azimuth and Elevation..... | 77 |
| Bibliography..... | 80 |

List of Figures

| Figure | Page |
|--|------|
| 1. Flux transfer from sun to satellite to detector..... | 8 |
| 2. Spectral radiance of a blackbody at $T=5900\text{ K}$ | 9 |
| 3. Source of area A_s emits into solid angle Ω_d subtended by detector. θ_d is the angle between the vector normal to the detector and the z-axis. | 11 |
| 4. Orientation of satellite with respect to sun scales apparent satellite size by $\cos(\theta_s)$ | 22 |
| 5. Convention for converting from spherical to rectangular coordinates | 24 |
| 6. Quantum efficiency as a function of wavelength for real and ideal photodetectors (Dereniak and Boreman, 1996:88) | 27 |
| 7. Background radiance from 833 cm^{-1} to 25000 cm^{-1} ($0.4\text{ }\mu\text{m}$ to $12\text{ }\mu\text{m}$) | 29 |
| 8. Atmospheric transmission from 833 cm^{-1} to 25000 cm^{-1} ($0.4\text{ }\mu\text{m}$ to $12\text{ }\mu\text{m}$) | 30 |
| 9. Solar spectrum at top of atmosphere generated by SOLAR 2000 | 33 |
| 10. Comparison of solar spectrum (black) and 5900 K blackbody (red)..... | 34 |
| 11. Comparison of SNR (black) and BLIP SNR (red) as a function of FOV from $1.2\text{ }\mu\text{m}$ to $1.3\text{ }\mu\text{m}$ | 43 |
| 12. Atmospheric transmission from 2500 cm^{-1} to 25000 cm^{-1} ($0.4\text{ }\mu\text{m}$ to $4.0\text{ }\mu\text{m}$) | 49 |
| 13. Background radiance from 2500 cm^{-1} to 25000 cm^{-1} ($0.4\text{ }\mu\text{m}$ to $4.0\text{ }\mu\text{m}$) | 50 |
| 14. SNR for 500-nm bands centered from $0.75\text{ }\mu\text{m}$ to $4.75\text{ }\mu\text{m}$ | 51 |
| 15. SNR for 100-nm bands centered from $0.45\text{ }\mu\text{m}$ to $4.95\text{ }\mu\text{m}$ | 51 |
| 16. SNR as a function of FOV for $0.6\text{-}0.7\text{ }\mu\text{m}$ (black), $0.8\text{-}0.9\text{ }\mu\text{m}$ (red), and $1.0\text{-}1.1\text{ }\mu\text{m}$ (green), and $1.2\text{-}1.3\text{ }\mu\text{m}$ (blue) for 100-nm wide bands | 53 |
| 17. Radiance of reflected sunlight (black) and blackbodies of 500 K (red) and 600 K (green) | 57 |
| 18. Atmospheric transmission for different visibility levels: 50.0 km (black), 23.0 km (red), 5.0 km (green) | 57 |
| 19. SNRs for 100-nm bands centered from $0.55\text{ }\mu\text{m}$ to $2.45\text{ }\mu\text{m}$ for visibilities of 50.0 km (black), 23.0 km (red), 5.0 km (green) | 58 |
| 20. SNRs over 100-nm bands centered from $0.55\text{ }\mu\text{m}$ to $2.45\text{ }\mu\text{m}$ for different aerosol environments: rural (green), urban (black), desert (red), maritime (blue)..... | 59 |

| Figure | Page |
|--|------|
| 21. SNRs for 100-nm bands centered from 0.55 μm to 2.45 μm for altitudes of 0 km (black), 1 km (red), 2 km (green), and 3 km (blue) | 61 |
| 22. Atmospheric transmission for detector pointed 30° (green), 60° (red), and 90° (black) from horizon for the sun with zenith angle 51.93° and azimuth -168.46° | 62 |
| 23. Background radiance for detector pointed 30° (green), 60° (red), and 90° (black) from horizon for the sun with zenith angle 51.93° and azimuth -168.46° | 62 |
| 24. SNRs for 100-nm bands centered from 0.8 μm to 1.7 μm for detector pointed at 30° (green), 60° (red), and 90° (black) from horizon for the sun with zenith angle 51.93° and azimuth -168.46° | 63 |

List of Tables

| Table | Page |
|---|------|
| 1. Typical values of parameters for common PV detectors (Dereniak and Boreman, 1996:94) | 28 |
| 2. List of parameters used to determine SNR for planar diffuse satellite | 38 |
| 3. Parameter list for small signal noise approximation..... | 42 |
| 4. Parameter list for BLIP approximation | 44 |
| 5. Values of parameters used to validate SNR model | 48 |
| 6. Detector parameters and SNRs for InGaAs PIN photodetectors at $T = 77\text{ K}$ | 55 |

RADIOMETRIC ANALYSIS OF DAYTIME SATELLITE DETECTION

I. Introduction

Space situational awareness (SSA) is essential for the Air Force's expanding role in the control and exploitation of space (Singer, 2004:2). The Air Force is currently seeking new ways to protect friendly space assets and continuously track space objects. The most favorable conditions for passive satellite detection and tracking exist when the satellite is illuminated by the sun but the detector on the ground is in the earth's shadow. These favorable conditions are limited to a few hours each day.

A 1983 study in support of Ground-based Electro-Optical Deep Space Surveillance (GEODSS) reports that "if low altitude satellites could be detected in the daytime by an electro-optical sensor, it would mean that it could do some of the work of large and expensive satellite tracking radars which are at few locations," (Rork, 1983: 103). The capability to detect and track satellites during the daytime will extend the time over which orbit information can be collected and will provide more frequent updates and more timely awareness of changes in satellite orbits.

Daylight detection of satellites is a complex problem. An end-to-end radiometric model of the detection process can be used to develop optimal daylight detection systems. In order to understand the requirements of such a model, it is important to understand some of the advances already made in daytime detection and modeling.

Literature Review

A review article published in *Instruments and Experimental Techniques* in 1999 discusses several infrared (IR) satellite detection systems demonstrated to work in daylight between 1962 and 1999. The satellite detection systems described can be divided into two categories. The first type of system is designed to detect sunlight reflected off of satellites and the second detects thermal emissions from satellites in the earth's shadow.

Daytime Star Detection.

In a 1962 paper, F. F. Hall and C. V. Stanley describe a nighttime detection system that detects reflected sunlight and some thermal emission from satellites. The system is also used to detect stars in the daytime. The system detected flux in two wavelength bands, with a PbS photoresistor for the 1-3- μm band and an InSb photodetector for the 2-6- μm band. A 1245-mm focal length Newton telescope with a 508-mm diameter principal mirror was used to collect light (Hall and Stanley, 1962:97). In the daytime, stars of magnitude $m = 3$ were detected with a θ_{FOV} of 1° (Hall and Stanley, 1962:102). Satellite detection with this system was limited to time periods when the detector was in twilight but the satellite was illuminated by the sun.

Daytime Detection of Satellites by Reflected Sunlight.

In 1983, successful demonstration of daytime satellite detection was described by E. W. Rork *et al.* The system was developed and demonstrated for the Air Force as part of GEODSS. A silicon photoconductive detector was used with a large, 31-inch diameter, 3937-mm focal length telescope and a small, 3-cm diameter, 150-mm focal length telescope (Rork, 1983: 104). The silicon detector used was sensitive between 0.35 μm and 1.1 μm , but a Kodak Wrattan No. 87 filter was used to block light with wavelengths

less than $0.8\ \mu\text{m}$. The TV camera rate was 30 frames per second, and the average quantum efficiency of the detector was 0.64 (Rork, 1983: 105). The system was validated by observing Polaris with the small telescope in the daytime with a signal-to-noise ratio (SNR) of 6 (Rork, 1983: 106). The large telescope was used to observe and track 18 satellites with a limiting magnitude of $m = 8.3$ (Rork, 1983: 103).

Daytime Detection of Satellites by Thermal Emission.

Another type of detection system was used to detect thermal emission from satellites in the earth's shadow. Thermal emission is primarily due to reflection of the earth's thermal radiation off the satellite's surface (Grishin, 1999: 5). Detectors for these types of systems are typically sensitive for longer wavelengths than those used for detecting reflected sunlight. M. J. Cantella *et al.* demonstrated a daytime detection system designed to detect satellites in the earth's shadow. The PtSi arrays used operated between 3.0 and $5.5\ \mu\text{m}$ (Grishin, 1999: 5), which was sufficient to detect reflection of the earth's thermal emission. This type of detection is also useful because the background radiation in this band is similar for day and night (Grishin 1999: 6). This system was used to detect and track more than 40 satellites in the daytime and nighttime (Grishin 1999: 6).

Reports of successful detection of stars and satellites in the daytime demonstrate that such systems can be built and operated. The second portion of the problem, and perhaps the more difficult question to answer, is how to optimize such systems in order to achieve daylight detection at low cost. The best way to investigate the parameters involved in the detection system is to model the system. An example of publications that demonstrate radiometric modeling is discussed below.

Radiometric Modeling.

In a 1988 paper, Richter and Fries describe a radiometric model of a detection system, as well as a computer program, that scans the spectral region to find the band center and bandwidth that produce the largest SNR (Richter and Fries, 1988:4771). Their model takes the SNR to be the ratio of total target flux density at the sensor to the noise equivalent flux density, which takes into account shot noise, thermal noise, generation-recombination noise, and one-over-f noise (Richter and Fries, 1988:4772). The authors account for atmospheric attenuation with atmospheric models generated by LOWTRAN, an Air Force Research Laboratory atmospheric modeling code. In this paper, Richter and Fries develop a robust SNR equation for IR detection systems. The equations presented can be adapted to the daylight scenario by including atmospheric modeling to account for background radiation and by accounting for the radiometric transfer of flux from the sun to the satellite to the detector.

Problem Statement

Although daytime satellite detection has been demonstrated and some radiometric models exist, the literature does not describe an end-to-end radiometric model that is adaptable to different observing conditions and different satellites. Examples of actual daytime detection described in the literature are difficult to compare because there are so many parameters involved. A robust model would allow different detection systems to be compared and parameters to be optimized. A model that incorporates daylight atmospheric transmission and background data, and that includes detection noise as well as background noise, would provide realistic analysis of existing or proposed systems.

The model developed as part of this research may be used to answer the following questions: What parameters affect the SNR in a daytime satellite detection system? How do these parameters affect the SNR? What are optimal and limiting atmospheric conditions for daytime satellite detection? What wavelength bands are best for observing satellites in the daytime?

Research Approach

The goal of this research is to determine which parameters influence the ability to detect a satellite in the daytime and how these parameters affect the detection system. This is accomplished by developing an end-to-end radiometric model of a detection system. Input parameters include date, time, location of the observer, atmospheric conditions, characteristics of the optics, characteristics of the detector, and characteristics of the satellite. For given input parameters, the SNR is calculated and used to determine whether or not the satellite can be detected.

The model is also used to determine the dependence of the SNR on several variables in order to determine which system parameters have the greatest impact on detection. Data obtained from this model is used to predict ideal observing conditions for daytime satellite detection.

Organization

A basic understanding of radiometry is required to develop the SNR equation. This background is provided in Chapter II. Chapter III discusses each variable in the SNR equation in greater detail and describes the methods used to determine values for each variable. Chapter IV presents analysis and results found by exercising the model for

various conditions. Chapter V provides conclusions and suggestions for future research in the area of radiometric models of daytime satellite detection systems.

II. Radiometry and Detection Background

In this chapter, basic background theory of radiometry and detection is presented. Radiometric terms and units are defined. The general SNR equation for daylight signal detection is developed and presented.

Radiometric process

The system of satellite detection follows the propagation of electromagnetic (EM) radiation from the sun to the detector as shown in Figure 1. A small fraction of the EM radiation emitted by the sun falls incident on the satellite. The amount of radiation incident on the satellite depends on the size, shape, and distance from the sun of the satellite. A fraction of that incident radiation, determined by material properties of the satellite, is reflected off of the satellite. This is added to radiation emitted from the satellite itself, as well as reflected earthshine. The combined radiation, consisting of reflected sunlight, reflected earthshine, and radiation from the satellite, is attenuated by scattering and absorption in the atmosphere. A fraction of the radiation that persists through the atmosphere falls onto the detector as signal.

Terms and Units

To begin, it is important to define terms and units used to calculate radiative emission, transfer, and detection. Radiative power, or flux (Φ), may be given in watts or in photons per second. Variables including flux in watts are denoted by a subscript, e , while variables including flux in photons per second are denoted by a subscript, q . Radiometric quantities introduced in this paper are spectral, that is, they are given as functions of wavelength or optical frequency. Typical units for optical wavelengths are

nm or μm . Units of optical frequency in wavenumbers are cm^{-1} . Wavelength is related inversely to wavenumbers, but the terms wavelength-dependent, wavenumber-dependent, and optical frequency-dependent, are used interchangeably throughout this paper. Finally, the source refers to the object emitting radiation and the detector refers to the object of interest upon which radiation falls. For example, in the calculation of flux from the sun incident on a satellite, the source refers to the sun and detector refers to the satellite. In the calculation of flux transferred from the satellite to a detector on earth, the source refers to the satellite and the detector refers to the actual detector on the ground.

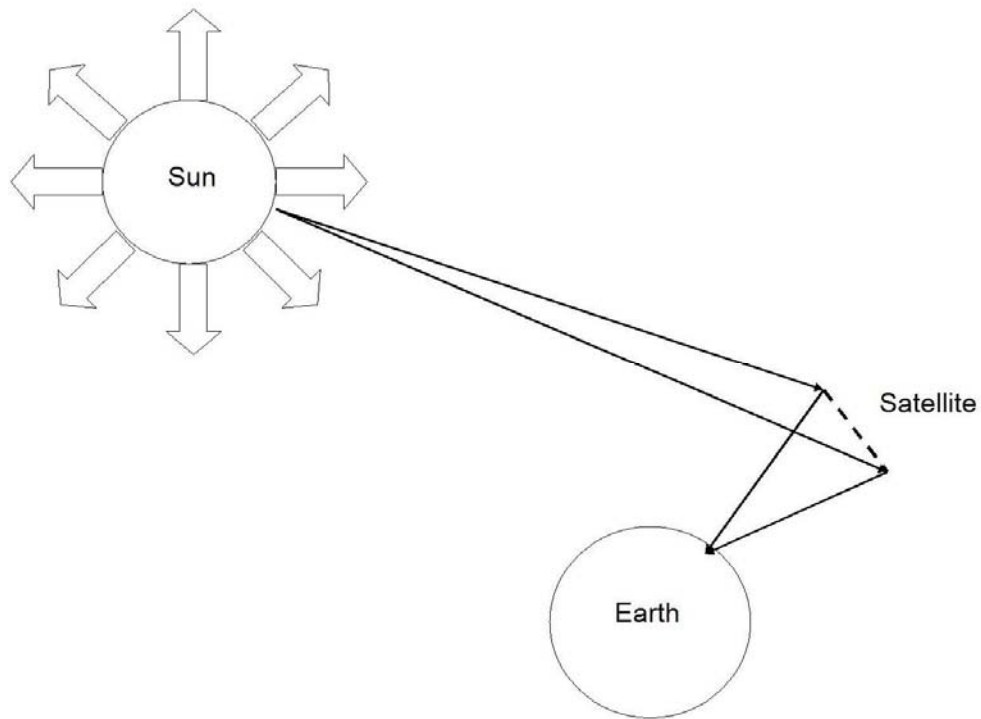


Figure 1: Flux transfer from sun to satellite to detector

Radiance.

Radiance is a material parameter that describes the power emitted by a source. This research considers sources that are blackbody sources or may be closely approximated by blackbody sources. Blackbody sources are perfect radiators, and their radiance as a

function of wavelength can be described if the temperature of the blackbody is known.

The spectral radiance of a blackbody is given by:

$$L_e(\lambda, T) = \frac{2hc^2}{\lambda^5 (\text{Exp}[\frac{hc}{\lambda kT}] - 1)} \left[\frac{W}{\text{cm}^2 \text{Sr} \mu\text{m}} \right], \quad (1)$$

where h is Planck's constant, c is the speed of light in a vacuum, λ is wavelength, k is Boltzmann's constant, and T is the temperature of the source in kelvins (Dereniak and Boreman, 1996: 56, 72). A graph of the spectral radiance of a blackbody is shown in Figure 2.

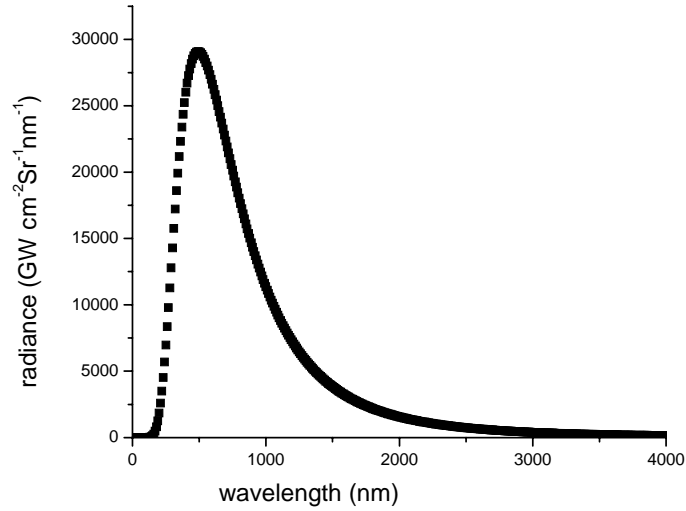


Figure 2: Spectral radiance of a blackbody at T=5900 K

Wein's Displacement Law.

The peak wavelength corresponds to the maximum radiance of a blackbody source and is given by Wein's displacement law:

$$\lambda_{peak} = \frac{2898}{T} \quad [\mu m], \quad (2)$$

where T is the temperature of the blackbody in kelvins and the resulting peak wavelength is in μm (Dereniak and Boreman, 1996:70). Peak wavelength decreases with increasing temperature. The peak wavelength of the 5900 K blackbody shown in Figure 2 is 0.49 μm .

Flux.

Generally, radiation is measured in terms of power or flux in units of watts. Flux depends on the geometry of the source and the solid angle over which the radiation is measured. Flux is given by

$$\Phi_e = \int_{\Omega_d} \int_{A_s} L_e \cos(\theta_s) \partial A_s \partial \Omega_d \quad \left[\frac{W}{\mu m} \right], \quad (3)$$

and so

$$L_e = \frac{\partial^2 \Phi_e}{\partial A_s \cos(\theta_s) \partial \Omega_d} \quad \left[\frac{W}{cm^2 Sr \mu m} \right], \quad (4)$$

where Φ_e is flux, A_s is the area of the source, Ω_d is the solid angle from the source subtended by the area of the detector, and θ_s is the tilt angle of the source (Dereniak and Boreman, 1996:45). Geometry of a simple radiometry problem is depicted in Figure 3.

Solid Angles.

Solid angles are measured in steradians (Sr) and are defined as the ratio of a surface area of a sphere to the square of the radius of the sphere. The solid angle of a

hemisphere, for example, is given by the ratio of half of the surface area of a sphere to the radius of the sphere, which is 2π Sr. The solid angle is given by

$$\partial\Omega = \frac{\partial A}{r^2} \quad [\text{Sr}], \quad (5)$$

where r is the radius of the sphere and ∂A is given in spherical coordinates as $r^2 \sin(\theta) d\theta d\phi$ and is the surface area of the portion of the sphere that subtends the solid angle (Dereniak and Boreman, 1996:39). If r^2 is much greater than A , then the small angle approximation may be applied and the surface area of the sphere may be approximated as the area of the plane perpendicular to the radius of the sphere. This is the paraxial approximation, which will be used throughout this paper.

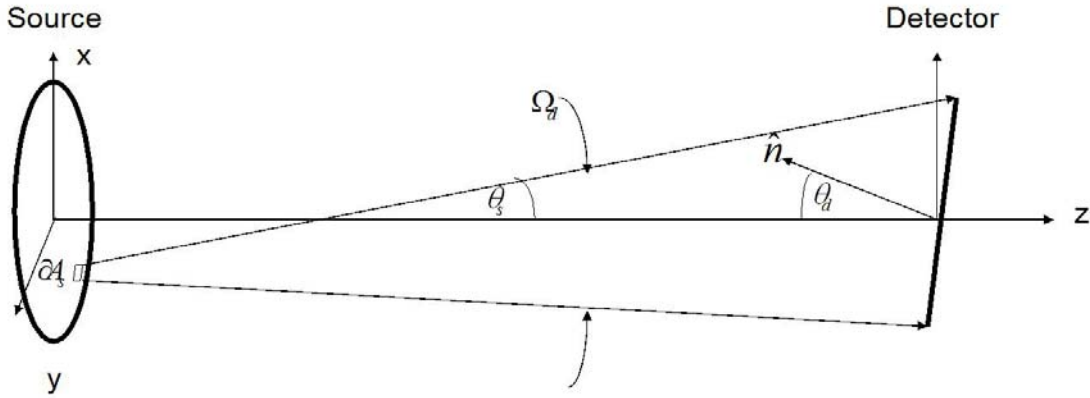


Figure 3: Source of area A_s emits into solid angle Ω_d subtended by detector. θ_d is the angle between the vector normal to the detector and the z-axis.

There are two solid angles of interest in radiometry. The first is given in differential form by $\partial\Omega_d = \partial A_d \cos(\theta_d)/R^2$ and is the solid angle from the source subtended by the detector, where R is the distance between the source and detector. The second is the FOV angle, Ω_{FOV} , given in differential form by $\partial\Omega_{\text{FOV}} = \partial A_s \cos(\theta_s)/R^2$. Ω_{FOV} is the solid angle

from the detector subtended by the source. In this paper, when FOV is given in radians, it is the square root of the solid angle and is denoted by θ_{FOV} .

Exitance.

Exitance is the measure of flux leaving a source per unit area of the source:

$$M_e = \frac{\partial \Phi_e}{\partial A_s} = \int_{\Omega_d} L_e \cos(\theta_s) \partial \Omega_d \left[\frac{\text{W}}{\text{cm}^2} \right], \quad (6)$$

where A_s is the area of the source (Dereniak and Boreman, 1996:46). Spectral exitance is the measure of flux per unit area leaving a source per unit wavelength, and is given by Equation (6) when flux is a function of wavelength.

Irradiance.

Irradiance is the measure of flux incident on a source per unit area of the detector and is given by the following equation:

$$E_e = \frac{\partial \Phi}{\partial A_d} = \int_{A_s} \frac{L_e \cos(\theta_s) \cos(\theta_d)}{R^2} \partial A_s \left[\frac{\text{W}}{\text{cm}^2} \right], \quad (7)$$

where A_d is the area of the detector, R is the distance between the source and detector, θ_d is the tilt angle of the detector and θ_s is the tilt angle of the source as shown in Figure 3 (Wolfe and Zissis, 1989:1-4).

The discussion and equations so far provide enough information to determine radiation emitted from a blackbody of known temperature for any range of wavelengths. In order to determine the SNR of the signal transmitted from the sun to the satellite to a detector on the earth's surface, more parameters are necessary.

Signal-to-Noise Ratio

The SNR is the ratio of the signal received by the detector to the total noise produced by the signal, background, and detector. The SNR can be described as the ratio of the signal current to the noise current (Richter and Fries, 1988: 4771). Noise adds in quadrature, and the resulting SNR can be expressed as

$$\frac{S}{N} = \frac{Signal}{\sqrt{Noise_{Signal}^2 + Noise_{Background}^2 + Noise_{Detector}^2}}, \quad (8)$$

where *Signal* is the current or voltage detected due to the target, *Noise_{Signal}* is the current or voltage noise due to the target, *Noise_{Background}* is the current or voltage noise due to the background, *Noise_{Detector}* is the noise in the detector, itself. The types of noise present in the detector depend on the detector type.

Flux may be given in watts or photons per second. The flux used in the SNR equation is a photon rate, so that multiplication by the quantum efficiency in electrons per photon and the charge per electron will produce units for current. The photon rate is converted to watts by multiplying by hc/λ joules per photon. This introduces wavelength dependence in the signal and noise terms.

Signal.

If the signal used in Equation (8) is the signal current, it is the product of the photon irradiance on the detector, the collecting area, and the quantum efficiency of the detector, modified by an efficiency parameter. Signal current can be calculated using the equation

$$Signal = E_{q-signal}^{opt} \cdot A_o \cdot \eta \cdot q \quad [A], \quad (9)$$

where $E_{q-signal}^{opt}$ is the total photon irradiance that falls on the optic given in photons per second per square meter, A_o is the area of the collecting optic in square meters, η is the quantum efficiency, and q is the charge per electron (Richter and Fries, 1988:4772).

Input parameters are given in terms of energy flux rather than photon flux, so photon irradiance is replaced by energy irradiance divided by hc/λ joules per photon.

Additionally, not all of the photons that reach the optics will propagate to the detector due to non-ideal transmission of the optics and filters used. When these additional parameters are considered and irradiance is measured in watts, the total signal across some band of optical frequency is given by

$$Signal = \frac{k_o q A_o}{hc} \int_{\nu_1}^{\nu_2} \eta(\nu) \cdot \tau_o(\nu) \cdot \tau_f(\nu) \cdot \tau_{atm}(\nu) \cdot E_{e-sig}^{opt}(\nu) \cdot \frac{1}{\nu^3} d\nu \quad [A], \quad (10)$$

where k_o is an efficiency term of the electronics, $\eta(\nu)$ is the quantum efficiency as a function of optical frequency in wavenumbers ν , $\tau_o(\nu)$ is the transmission coefficient of the optics, $\tau_f(\nu)$ is the transmission coefficient of the filter, $\tau_{atm}(\nu)$ is the transmission coefficient of the atmosphere, and $E_{e-sig}^{opt}(\nu)$ is the irradiance from the target at the optic (Richter and Fries, 1988: 4772). Quantum efficiency, irradiance, and the transmission coefficients are all dependent on optical frequency and must be integrated over the bandwidth to determine total irradiance on the detector.

Noise.

Noise contributions, in general, are random fluctuations in the signal. This occurs when the signal is present and when it is not. Shot noise in a photovoltaic detector results from the random arrival of photons at the detector (Dereniak and Boreman, 1996:173).

Shot noise comes from both the photons produced by the target and the photons produced by the background. Thermal noise results from the random excitation of electrons within the detector when the detector is at some temperature greater than absolute zero (Dereniak and Boreman, 1996:168). Generation-recombination noise occurs because the rate of generation and rate of recombination of carriers have inherent uncertainty (Dereniak and Boreman, 1996:174). One-over-f noise is not well understood, but is observed to increase with decreasing electrical frequency of the detector (Dereniak and Boreman, 1996:183). In thermal detectors, uncertainty in measured temperature is called temperature noise (Dereniak and Boreman, 1996:177).

Signal shot noise.

Signal shot noise is shot noise due to the random arrival at the detector of photons produced by the target. In the case of daytime satellite detection by a single detector, the number of photons produced by the target is so much smaller than the number of photons produced by the background that signal noise can be ignored. It is included in the model for completeness, but can be approximated as zero in order to simplify the SNR equation when determining dependence on different variables. Unless specified otherwise, however, the signal noise is included in all runs of the model.

Signal shot noise is given by the equation

$$Noise_{Signal} = \left(\frac{2A_o q^2 \Delta f}{hc} \int_{\nu_1}^{\nu_2} \eta(\nu) \tau_o(\nu) \tau_f(\nu) \tau_{atm}(\nu) E_{e-sig}^{opt}(\nu) \frac{1}{\nu^3} d\nu \right)^{1/2} [A], \quad (11)$$

where Δf is the noise equivalent bandwidth in Hz.

Background shot noise.

Background shot noise is additional shot noise due to the random arrival of photons at the detector from the background. Background shot noise is given by

$$Noise_{background} = \left(\frac{2A_o q^2 \Delta f}{hc} \int_{\nu_1}^{\nu} \eta(\nu) \cdot \tau_o(\nu) \cdot \tau_f(\nu) \cdot E_{e-back}^{opt}(\nu) \frac{1}{\nu} d\nu \right)^{1/2} [A], \quad (12)$$

Background irradiance is the product of background radiance and Ω_{FOV} .

Detector noise.

Descriptions of detector noise depend on the type of detector used. In thermal detectors, incident flux raises the temperature of some temperature-sensitive element, which causes measurable change of another element in the detector. For example, in a bolometer, incident flux causes a temperature increase which causes a change in resistance, which can then be measured (Dereniak and Boreman, 1996:86). In photodetectors, which include photoconductive (PC) and photovoltaic (PV) detectors, incident photons generate electrons which can be effectively counted by measuring the change in some parameter. In PC detectors, the change in resistance or conductance is used to determine the incident flux. Generation-recombination noise is present in PC detectors. In PV detectors, incident photons induce a voltage or current. Thermal noise, also called Johnson noise, is present in PV detectors (Dereniak and Boreman, 1996:93).

Thermal noise, or Johnson noise, is caused by random excitation of electrons in a detector. For temperatures greater than absolute zero, carriers experience thermal motion and cause charge gradients across resistors (Dereniak and Boreman, 1996:168). Johnson noise is given by

$$Noise_{thermal} = \left(\frac{4 \cdot kT_d \cdot \Delta f \cdot A_d}{RA} \right)^{1/2} [A], \quad (13)$$

where T_d is the temperature of the detector in kelvins, A_d is the area of the detector in square meters, and RA is the resistance-area product (RA product) of the detector in Ohms-square meters. The RA product, rather than the resistance of the detector, is frequently listed as a detector parameter.

Generation-recombination noise occurs in photoconductors, where there is some gain associated with detection. Generation-recombination noise is due to uncertainty in the rate of generation and rate of recombination of carriers in the detector. Generation-recombination noise is given by

$$Noise_{g-r} = 2qG(\eta E_q^{det} A_d \Delta f + g_{th} A_d \Delta f l_x)^{1/2} [A] \quad (14)$$

where G is the photoconductive gain, E_q^{det} is the photon irradiance at the detector due to the signal and the background, g_{th} is the thermal generation of carriers, and l_x is the thickness of the detector in the direction of optical propagation (Dereniak and Boreman, 1996:175).

One-over-f noise depends on the inverse of the modulation frequency. One-over-f noise is given by

$$Noise_{1/f} = \left(\frac{B \cdot I^\alpha}{f^\beta} \right)^{1/2} [A], \quad (15)$$

where I is the rms current in Amperes, f is the modulation frequency in Hz, α is empirically determined to be near two, β is empirically determined to be near one, and B is an empirically determined proportionality constant (Dereniak and Boreman, 1996:183). For the purpose of this research, B will be kept at zero and one-over- f noise will be ignored. This approximation is certainly valid for large detector frequencies.

Temperature noise occurs in thermal detectors and is due to the uncertainty of the temperature measured by the detector (Dereniak and Boreman, 1996:179). Temperature noise is given by

$$Noise_{temp} = \left(\int_0^{\infty} \frac{4kKT^2}{K^2 + (2\pi f)^2 H^2} df \right) = \frac{kT^2}{H} \quad [K] \quad (16)$$

where K is thermal conductance in W/K and H is heat capacity in J/K, (Dereniak and Boreman, 1996:181-182).

Signal-to-Noise Ratio Equation.

In this research, analysis is limited to detection by a PV detector. In this case, detector noise is due to thermal noise and one-over- f noise. The final equation used to determine SNR for a PV detector is found by putting together the definitions given for the signal, signal shot noise, background shot noise, thermal noise, and one-over- f noise above:

$$SNR = \frac{\frac{k_o q A_o}{hc} \int_{\nu_1}^{\nu_2} \eta \tau_o \tau_f \tau_{atm} E_{e-sig} \frac{1}{\nu^3} d\nu}{\sqrt{\frac{2q^2 A_o \Delta f}{hc} \left(\int_{\nu_1}^{\nu_2} \eta \tau_o \tau_f \tau_{atm} E_{e-sig}^{opt} \frac{1}{\nu^3} d\nu + \Omega_{FOV} \int_{\nu_1}^{\nu_2} \eta \tau_o \tau_f L_{e-back} \frac{1}{\nu^3} d\nu \right) + \frac{4kT_d A_d \Delta f}{RA} + \frac{BI^2}{f}}} \quad (17)$$

Parameters inside the integrals are dependent on optical frequency, while parameters outside the integrals are constant with respect to optical frequency.

Summary

This chapter discussed general principles of radiometry and the SNR equation. The next chapter will go into greater detail about the variables included in the SNR equation and how they are found or calculated. The next chapter will also discuss approximations that may be made to the SNR equation.

III. Modeling

Background theory presented in the previous chapter built the SNR equation from radiometry principles. In this research, analysis was limited to detection by a photovoltaic detector. Therefore, in this chapter, each of the variables in the SNR equation associated with photovoltaic detection will be discussed. Some initial constraints must be taken into consideration before the remaining parameters can be analyzed. If the system under consideration is to consist of commercial off-the-shelf components, there are limits to the size and quality of the components. These constraints determine the range of the variables in the SNR equation. Additionally, some assumptions will be made regarding the optical-frequency-dependence of parameters in order to simplify the model. Finally, approximations to the equation will be examined in order to determine the conditions under which the equation can be simplified.

Signal Irradiance

The most important parameter that contributes to signal is signal irradiance, (E_{e-sig}^{opt}), given in units of power per unit area. Signal irradiance is found by determining the fraction of flux per unit area leaving the sun that is intercepted by the satellite, reflected off the satellite, and allowed to pass through the atmosphere to be detected by the collecting optic. It depends on solar radiance, reflectance of the satellite, and the geometry of the satellite with respect to the sun and the detector.

In order to ignore additional complications of the satellite's orientation, a planar diffuse satellite is used in this model. Additional research may adapt this model to include more realistic satellite designs and material properties. For a planar satellite, far

enough from the sun to justify the small angle approximation, the irradiance on the satellite is given by

$$E_{e-sat} = \frac{L_{e-sun} A_{sun} \cos(\theta_s)}{R_{sun-sat}^2} \left[\frac{W}{cm^2} \right], \quad (18)$$

where L_{e-sun} is the radiance of the sun, θ_s is the angle at which the satellite is oriented with respect to the sun, $R_{sun-sat}$ is the distance between the sun and the satellite which may be approximated as one astronomical unit (AU), or $1.50 \cdot 10^8$ km, and A_{sun} is the area of the sun when viewed as a disc. This approximation of the area of the sun is valid because the sun is viewed as a Lambertian source very far away from the satellite.

Since the satellite used in the model is assumed to be a diffuse reflector, it can also be treated as a Lambertian source, with exitance equal to the product of the irradiance falling on the detector and the reflectivity of the detector. For a Lambertian source, radiance is exitance divided by π , so the radiance of the satellite is

$$L_{e-sat} = \frac{\rho_{sat} L_{e-sun} A_{sun} \cos(\theta_s)}{\pi R_{sun-sat}^2} \left[\frac{W}{cm^2 Sr} \right], \quad (19)$$

where ρ_{sat} is the reflectance of the satellite material.

Now, the irradiance on the detection optic is the product of this new radiance and the area of the satellite, divided by the square of the distance between the satellite and the detector:

$$E_{e-sig}^{opt} = \frac{\rho_{sat} L_{e-sun} A_{sun} A_{sat} \cos(\theta_s)}{\pi R_{sun-sat}^2 R_{sat-det}^2} \left[\frac{W}{cm^2} \right], \quad (20)$$

where A_{sat} is the area of the satellite and $R_{sat-det}$ is the distance between the satellite and the detector.

Orientation Angle.

The angle between the vector normal to the plane of the satellite and the vector from the center of the sun to the center of the satellite determines the size of the satellite apparent to the sun. When the plane of the satellite faces the sun, the angle is zero. When the satellite is oriented at some nonzero angle with respect to the sun, the apparent size of the satellite is decreased by the cosine of the angle. This is illustrated in Figure 4.

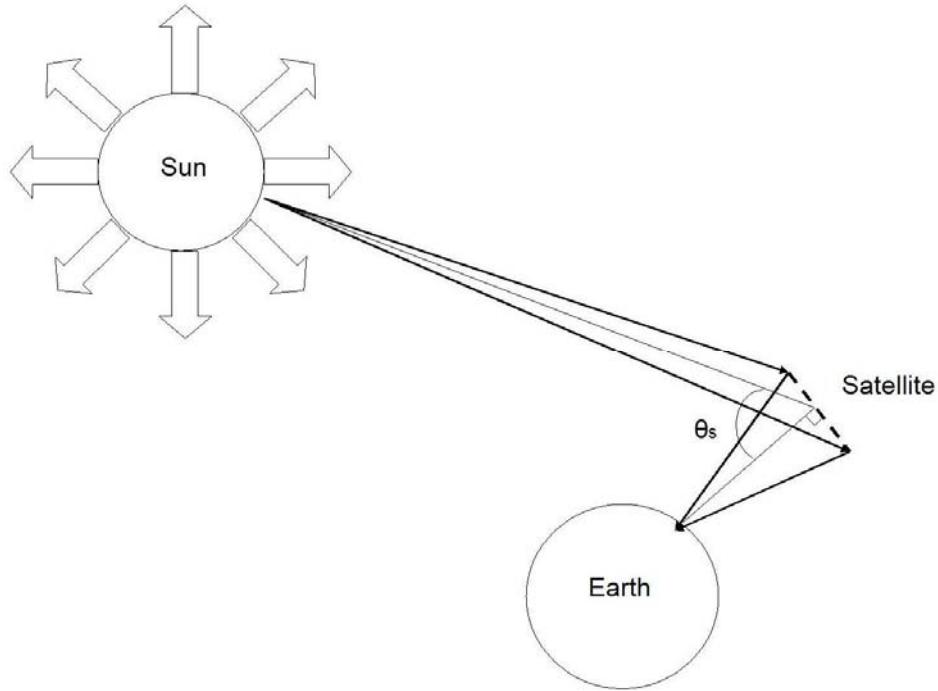


Figure 4: Orientation of satellite with respect to sun scales apparent satellite size by $\cos(\theta_s)$

The angle, θ_s , is the angle between a line drawn from the sun to the satellite and the line normal to the satellite's surface. This can be determined if the position of the sun and the position of the satellite, both relative to the observer, are known. The position of the

sun and satellite in the sky are given by zenith, (0° for an object directly overhead and 90° for an object on the horizon), and azimuth, (0° for an object due north, 90° for an object due east, 180° for an object due south, and 270° for an object due west). If both objects are considered to be on the surface of a unit sphere, then the spherical coordinates (r, θ, φ) of each are known, and the sun, satellite, and detector form the vertices of a triangle. The spherical coordinates can be transformed to rectangular coordinates (x, y, z) , and used to determine the distance between the sun and satellite. Then, the lengths of all three sides of the triangle are known, and the angle, θ_s , can be calculated.

Using the convention illustrated in Figure 5, the positive x axis is north, y is west, θ is the angle from zenith and φ is equal to the negative of the azimuth, since azimuth is measured from north clockwise, and φ is measured from the positive x axis counter-clockwise. The transformation from spherical coordinates to rectangular coordinates is given by the following equations for rectangular coordinates x , y , and z in terms of r , φ , and θ :

$$\begin{aligned} x(r, \varphi, \theta) &= r \cdot \sin(\theta) \cdot \cos(\varphi) \\ y(r, \varphi, \theta) &= r \cdot \sin(\theta) \cdot \sin(\varphi) , \\ z(r, \varphi) &= r \cdot \cos(\theta) \end{aligned} \tag{21}$$

where r is the radius of the sphere, in this case one for both the satellite and sun, θ is the zenith angle, and φ is the negative azimuth angle (Marsden and Tromba, 1996:371).

The orientation angle, θ_s , can be written as a function of the zenith and azimuthal angles of the sun and satellite

$$\theta_s = \cos^{-1} \left(\frac{\sqrt{(x(r, z_{sun}, a_{sun}) - x(r, z_{sat}, a_{sat}))^2 + (y(r, z_{sun}, a_{sun}) - y(r, z_{sat}, a_{sat}))^2 + (z(r, z_{sun}) - z(r, z_{sat}))^2}}{2} \right) \quad (22)$$

where the functions for x , y , and z are given in Equation (21), and r is equal to one.

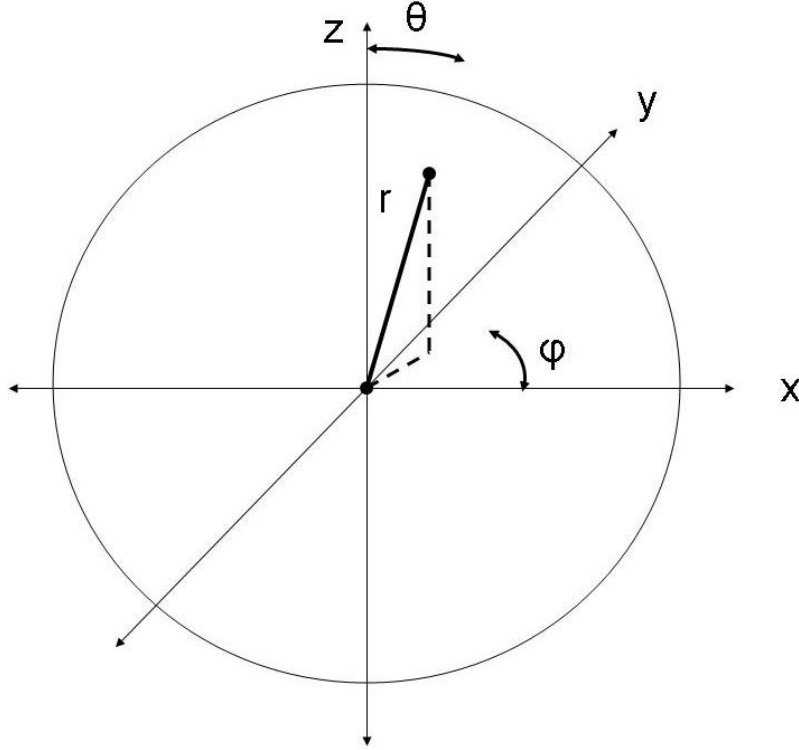


Figure 5: Convention for converting from spherical to rectangular coordinates

Other parameters affecting the signal

Spectral quantities are preferred in order to determine SNRs over different bandwidths and band centers. Solar radiance and the satellite's reflectivity are given as functions of wavenumber, and the calculated irradiance falling on the detector is a spectral quantity that must be multiplied by the wavenumber-dependent quantum efficiency and transmission coefficients in order to determine the total signal.

So far, this treatment ignores losses due to propagation through a medium. From the sun to the satellite, the signal travels through a vacuum and experiences approximately no losses. From the satellite to the detector at the earth's surface, however, the signal is attenuated by the atmosphere. This attenuation can be expressed as a spectral atmospheric transmission coefficient, which ranges between zero and one.

Transmission of atmosphere

Attenuation due to the atmosphere is wavenumber-dependent and varies widely over the bands investigated in this model. The transmission coefficients used in this model were provided by the Phillips Laboratory Expert-assisted User Software, (PLEXUS), which employs MODTRAN and FASCODE transmission codes. In addition to wavenumber, transmission through the atmosphere depends on many other parameters. The quality of the atmosphere and densities of different types of particles which absorb and scatter in different bands vary with weather, pollution levels, time of day, and season. The altitude of the observer and the observer-satellite zenith angle determine how much atmosphere exists between the detector and the satellite. Detecting satellites closer to the horizon requires the signal to pass through more of the atmosphere, causing greater attenuation and a smaller SNR, while detecting from high altitudes increases SNR by limiting the atmosphere through which the signal must travel. The position of the sun with respect to the satellite is also a factor, because a brighter sky near the sun contributes more background noise and diminishes the SNR.

Transmission of optics

The transmission of the optics is an important parameter that can severely limit the signal that reaches the detector. Real systems have a wavenumber-dependent optical

transmission between zero and one. For the purpose of this research, optical transmission is treated as a scalar constant between zero and one.

Transmission of filters

The optical transmission of the filter is wavelength-dependent. It is near zero for wavelengths above and below the maximum and minimum wavelengths, respectively, and takes on values near one within the band. As for the optical transmission, filter transmission is not ideally one and will attenuate the signal before it reaches the detector, limiting the SNR. Although there is some wavenumber dependence of transmission through the filter, a well-designed filter will have a nearly constant transmission across the band for which it is designed. It is a valid approximation to treat the transmission of the filter as a scalar constant.

Quantum efficiency

Quantum efficiency is the ratio of the electrons generated for each photon incident on the detector (Dereniak and Boreman, 1996:87). It ranges between zero and one, and does not account for additional electrons produced within the detector. These additional electrons are considered in a separate gain term. Quantum efficiency is wavelength dependent. Ideal photodetectors have a constant quantum efficiency of one up to some cutoff wavelength, but real detectors tend to have a quantum efficiency that is less than one and decreases for wavelengths near zero and near the cutoff wavelength, as shown in Figure 6 (Dereniak and Boreman, 1996:88). The cutoff wavelength is the wavelength which corresponds to an energy equal to the bandgap energy of the semiconductor material of which the detector is made. Incident photons of longer wavelengths do not carry enough energy to overcome the bandgap and do not produce electrons.

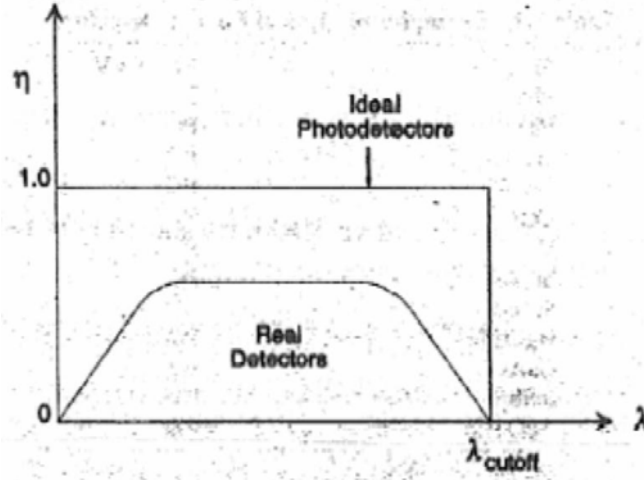


Figure 6: Quantum efficiency as a function of wavelength for real and ideal photodetectors (Dereniak and Boreman, 1996:88)

Quantum efficiency is given by the equation

$$\eta(\lambda) = (1 - r_{Fres})(1 - e^{-al_x}), \quad (23)$$

where r_{Fres} is the Fresnel reflectance of the detector material, a value between zero and one, a is the absorption coefficient, and l_x is the absorption path length (Dereniak and Boreman, 1996:89). Near the cutoff wavelength, absorption is proportional to the square root of the difference between the energy of the photon and the bandgap energy. As the wavelength of the incident photon increases toward the cutoff wavelength, this difference decreases and the resulting absorption approaches zero. This causes the quantum efficiency to decrease for wavelengths near the cutoff wavelength (Dereniak and Boreman, 1996:88). The Fresnel coefficient for normal incidence is given in terms of refractive index of the material, $n(\lambda)$, by

$$r_{Fres}(\lambda) = \frac{(n(\lambda) - 1)^2}{(n(\lambda) + 1)^2}, \quad (24)$$

(Dereniak and Boreman, 1996:29). Since for most materials used to make photovoltaic detectors, the refractive index increases with decreasing wavelength, the Fresnel coefficient decreases as the wavelength of the incident photon decreases toward zero, causing the quantum efficiency to drop off for very short wavelengths.

Some typical values for quantum efficiency are given in Table 1. If the bandwidth of interest is well above zero and well below the cutoff wavelength, the quantum efficiency can be approximated as a wavelength-independent parameter.

Table 1: Typical values of parameters for common PV detectors (Dereniak and Boreman, 1996:94)

| Material | quantum efficiency η [%] | detector type | resistance R_d [Ω] | cutoff wavelength λ_{cutoff} [μm] | operating temperature T [K] |
|-----------|-------------------------------|---------------|-------------------------------|---|-------------------------------|
| InSb | 45 | PV | 10^9 | 5.5 | 77 |
| HgCdTe | 65 | PV | 10^7 | 5 | 77 |
| InAs | 40 | PV | 10^8 | 3.3 | 77 |
| InGaAs | 86 | PV | 10^8 | 1.7 | 300 |
| PIN (Si) | 80 | PV | | 1.1 | 300 |
| Aval (Si) | 70 | PV | | 1.1 | 300 |
| GaAsP | 60 | PV | $13(10^8)<43(10^8)$ | 0.7 | 300 |
| Si | 65 | PV | $10^8<35(10^8)$ | 1.1 | 300 |
| Ge | 64 | PV | $10^4<10^6$ | 1.8 | 300 |

Wavelength and Wavenumber

The model draws input data from many sources, so it is a critical step to make the units agree. Wavenumbers, with units of inverse centimeters, are chosen to represent the optical frequency, because the atmospheric modeling tool used produces results for transmission and background radiation as functions of wavenumber. Within the model, inverse centimeters are converted to inverse meters so that wavenumber terms will agree with other SI values.

Ideal bands for detecting solar reflectance were determined by running the model for different bands falling between 833 cm^{-1} and 25000 cm^{-1} ($0.4\text{ }\mu\text{m}$ to $12\text{ }\mu\text{m}$). From initial runs, it was determined that the best region of the spectrum in which to look was between 2500 cm^{-1} and 25000 cm^{-1} ($0.4\text{ }\mu\text{m}$ to $4\text{ }\mu\text{m}$). Within the region between 833 cm^{-1} and 2500 cm^{-1} , the background radiation is too high and background noise overwhelms the signal, as shown in Figure 7. Within the visible range, 14285 to 25000 cm^{-1} , ($0.4\text{ }\mu\text{m}$ to $0.7\text{ }\mu\text{m}$), the signal is attenuated by low atmospheric transmission, as shown in Figure 8. A viewing angle of 45° and a θ_{FOV} of 70 mrad were used for these and all other atmospheric models used in this research unless otherwise stated. The sun was located with a zenith angle of 51.93° and an azimuthal angle of -198.46° , which corresponds to the location of the sun on 25 October 2005 at 1730 GMT for an observer in Dayton, OH, at 38.89°N and -77.01°E .

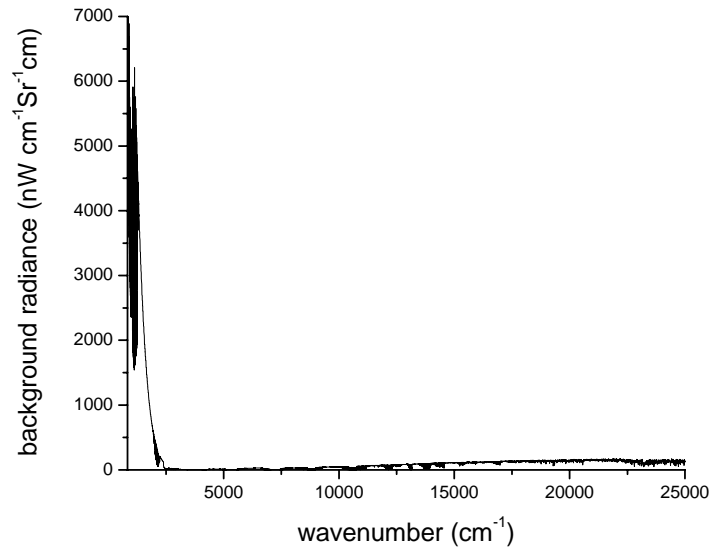


Figure 7: Background radiance from 833 cm^{-1} to 25000 cm^{-1} ($0.4\text{ }\mu\text{m}$ to $12\text{ }\mu\text{m}$)

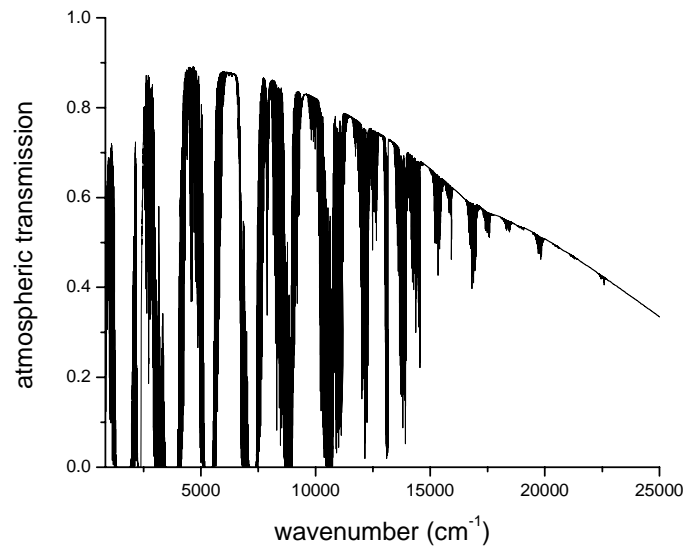


Figure 8: Atmospheric transmission from 833 cm^{-1} to 25000 cm^{-1} ($0.4 \text{ }\mu\text{m}$ to $12 \text{ }\mu\text{m}$)

Background radiance

Background radiance is given in units of watts per square meter per steradian per inverse centimeter. Background radiance as a function of wavenumber is provided by PLEXUS. As with atmospheric transmission, background radiance depends on atmospheric conditions including aerosol content, visibility, proximity to the sun, and thickness of the atmosphere between the satellite and observer.

Field of View

The FOV is a function of the optics and is given by the ratio of the area of sky observed to the square of the range. A smaller FOV improves the SNR by limiting the background radiation that reaches the detector. However, a smaller FOV limits the usefulness of the detection system by limiting the region of sky observed. In general, satellites can either be detected by scanning a wide region of sky until a satellite crosses the FOV, or the telescope can be pointed in the general vicinity of a satellite of known

orbit. The difference between these two modes of operation can be described as the difference between determining a satellite's orbit and verifying that a satellite is within a certain range of its expected orbit.

In a paper outlining order-of-magnitude estimates for parameters associated with daytime satellite detection, Bondar' and his associates claim that a θ_{FOV} of 20° (350 mrad) is necessary for locating satellites of unknown location, while a θ_{FOV} of only 1.5° (26 mrad) is necessary for verifying a satellite's location (Bondar', 1994:238). In this research, a θ_{FOV} of 4.0° (70 mrad) was used. This θ_{FOV} allows detection of a satellite that is approximately 7 km off orbit for every 100 km of altitude.

Optics

The desired detection system is relatively low-cost, mobile, and rapidly-deployable. In order to limit the optical mounting and equipment necessary, and to limit cost, a 16-inch diameter optic is chosen for the default value. This corresponds to an optical area of 0.1297 m^2 . An example of a commercially available 16-inch diameter telescope is the Meade 16-inch LX200GPS Schmidt-Cassegrain telescope. It has a focal length of 4064 mm, weighs 230 lbs, and costs approximately \$11,000 (Meade General Catalogue, 2004:1, Optics Planet, 2005:1). Optics that fit the criteria used to calculate SNRs for daytime detection are commercially available.

Reflectance of the Satellite

In order to simplify the SNR equation, the satellite surface is assumed to be diffuse or Lambertian, that is, light reflects off the surface in all directions, independent of the incident angle. The opposite extreme is a specular surface, which reflects in only one direction for a given incident angle. Most surfaces exhibit some combination of these two

extremes, and require empirically-derived, bi-directional reflectance distribution functions (BRDFs) to describe the dependence of reflectance on incident angle. Future research may include modifying this model to include a reflectance parameter for a more realistic surface.

To further simplify the SNR equation, the reflectance of the satellite is approximated to be independent of optical frequency. Real materials have reflectances that are wavenumber-dependent. The SNR equation can be easily adapted to wavenumber-dependent reflectance by allowing the reflectance function to modify the signal before the total signal is summed over the optical frequency band.

Solar Radiance

In order to evaluate the SNR over different bands, it is necessary to obtain a spectral solar radiance function. The solar spectrum used, provided by Space Environment Technologies, is valid for 19 Feb 1979. The solar spectrum varies little in the IR throughout the year, so the IR portion of the spectrum is a useful approximation for any day and time. The model is scaled for a sun that is 1 AU away from the sun.

The data from the SOLAR 2000 model was given in watts per square meter, for a range of wavelengths in nanometers, and is valid at the top of the earth's atmosphere. A graph of the data provided is shown in the Figure 9 (Space Environment Technologies, 2005:1)*.

The SNR equation requires the solar radiance to be a function of wavenumber, with units of watts per square meter per steradian per inverse centimeter. To convert the solar

* SOLAR2000 Research Grade historical irradiances are provided courtesy of W. Kent Tobiska and SpaceWx.com. These historical irradiances have been developed with funding from the NASA UARS, TIMED, and SOHO missions.

spectrum data given to spectral solar radiance at the sun, the irradiance is divided by the solid angle $6.76372 \cdot 10^{-5}$ Sr, which is the ratio of the area of the sun when treated as a disc to the square of the distance from the sun to the earth, for a solar radius of $6.96 \cdot 10^8$ m and the distance from the sun to the earth of 1 AU. This gives the solar radiance at the surface of the sun, but the values at each wavelength are still integrated over 1-nm bands.

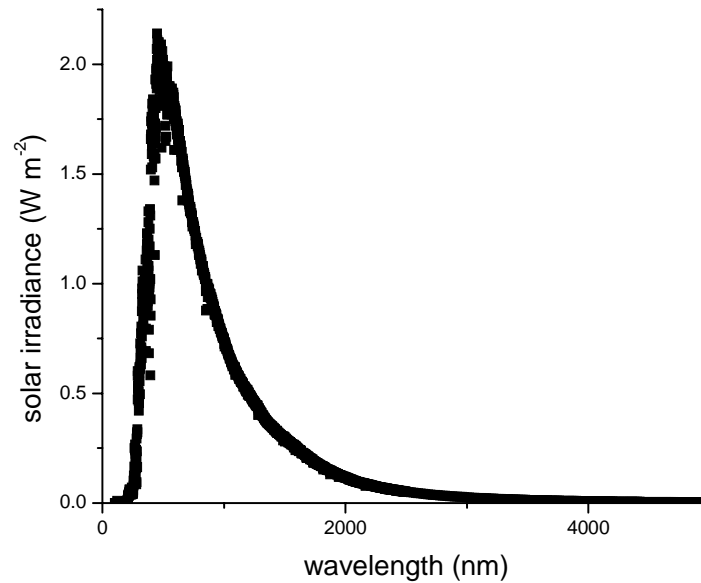


Figure 9: Solar spectrum at top of atmosphere generated by SOLAR 2000

To get the spectral solar radiance at the sun's surface, radiance is divided by 10^{-9} m to obtain spectral solar radiance at the sun with units of power per area per solid angle per wavelength. A graph comparing the calculated solar radiance to the blackbody curve for a blackbody of temperature 5900 K is shown in Figure 10.

Finally, the solar radiance must be converted to a function of wavenumber, in order to agree with the other functions in the SNR equation. This is accomplished by taking the reciprocal of each wavelength and converting to units of inverse centimeters. The data

was then interpolated in *Mathematica* to produce solar radiance as a function of wavenumber.

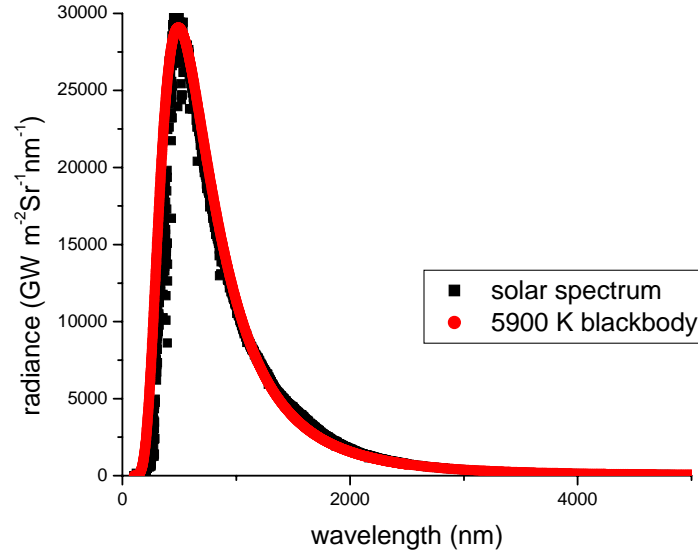


Figure 10: Comparison of solar spectrum (black) and 5900 K blackbody (red)

Angular extent of satellite

The solid angle subtended by the satellite is given by the ratio of the area of the satellite to the square of the distance from the satellite to the observer. These two variables are combined into a single parameter that describes the apparent size of the satellite. Satellites in a low-earth orbit (LEO) have orbits that range from 200 to 3000 km from the surface of the earth. Most satellites are on the order of meters in size. For a planar satellite that is 16 m^2 , the solid angular extent ranges from 40 nSr at 200 km to 1.8 pSr at 3000 km.

Noise-equivalent Bandwidth

The noise-equivalent bandwidth, Δf , measured in Hz, can be approximated as the inverse of the integration time. For LEO satellites, the integration time must be very

small because the satellite moves very quickly across the FOV. An integration time of 10 ms results in a noise-equivalent bandwidth of 100 Hz. When one-over-f noise is ignored, the SNR depends on noise-equivalent bandwidth to the negative one-half power, so larger bandwidths result in smaller SNRs.

Detector Parameters

IR detectors are divided into two major classes: photon detectors, in which incident photons interact with electrons to produce a measurable signal, and thermal detectors, in which incident radiation causes a change in temperature of the material to produce a measurable signal (Rogalski and Chrzanowski, 2002:114). Detectors considered in this paper are restricted to photon detectors, specifically semiconductor photovoltaic detectors sensitive in the visible and near IR regions of the spectrum (up to 5 μm). Photon detectors offer high efficiency and fast performance, but require cryogenic cooling which adds weight and cost (Rogalski and Chrzanowski, 2002:114). Common semiconductor detector materials and their cutoff wavelengths are listed in Table 1. Possible detector materials of use in daylight detection include InSb, InAs, InGaAs, Si, Ge, PbS, and PbSe.

Detector Noise.

Since one-over-f noise is ignored in this paper, the only detector noise is Johnson noise, which depends on the noise-equivalent bandwidth, discussed above, and the temperature of the detector, the area of the detector and the RA product of the detector.

Detector Temperature.

Johnson noise depends linearly on the detector temperature. Cooler detector temperatures result in fewer thermally excited electrons and less thermal noise. The thermal noise for a detector at 300 K is nearly four times as high as that for the same

detector cooled to 77 K. For a Johnson-noise limited system, in which Johnson noise is dominates all other noises, a change in temperature from 77 K to 300 K would decrease the SNR by nearly 50%.

Detector Area and Resistance-Area Product.

Johnson noise depends on the resistance of the detector and not on the detector area, but manufacturers frequently characterize detectors by the RA product, given in $\Omega\text{-cm}^2$. In order to use this parameter in the denominator of the Johnson noise term, the detector area is included in the numerator. Johnson noise, then, depends on the detector area and on the inverse of the RA product. Larger detector areas produce greater noise, while larger RA products result in smaller levels of Johnson noise. The RA product can be found from the given dark current and detector area by combining the following equations for RA product and dark current:

$$RA = \frac{\beta_i k T_d n_a \tau_e}{q^2 l_n n_i^2} \quad [\Omega\text{cm}^2], \quad (25)$$

and

$$i_o = \frac{A_d q l_n n_i^2}{\tau_e n_a} \quad [A], \quad (26)$$

where τ_e is carrier lifetime, n_a is doping concentration, l_n is diffusion length, n_i is intrinsic carrier concentration, and β_i is a nonideality factor that can be approximated as one (Dereniak and Boreman, 1996:253, 256). In the nonideal case, β_i is larger than one.

These two equations can be combined to find the RA product in terms of detector temperature, detector area, and dark current, when β_i is equal to one:

$$RA = \frac{kT_d A_d}{qi_o} \quad [\Omega cm^2] \quad (27)$$

A G8423-05 Hamamatsu InGaAs PIN photodetector sensitive from 1.2 to 2.6 μm with an active area of 0.5 mm² and a dark current of 50 μA has a calculated RA product of 0.663296 $\Omega\text{-cm}^2$ (Hamamatsu Corporation, 2005:1).

If the RA product is substituted back into the equation for thermal noise (Equation 13), it becomes apparent that thermal noise can be written in terms of dark current and noise-equivalent bandwidth only.

$$Noise_{thermal} = (4qi_o \Delta f)^{1/2} \quad [A]. \quad (28)$$

The thermal noise is kept in terms of detector area and resistance-area product in the SNR equation because these are standard parameters frequently listed by manufacturers.

Variables with units and default values

A complete list of variables included in the SNR equation, along with the range of values the variables may take and the default values assigned to each variable, is included in Table 2. Constants such as Planck's constant, the speed of light, and the area of the sun are not included. The distance from the sun to the satellite is treated as a constant. The default values for the detector are for the Hamamatsu G8423-05 InGaAs PIN photodiode described above. The *Mathematica* code used to develop the daytime detection model and calculate the SNR for a given set of parameters is included in Appendix A.

Table 2: List of parameters used to determine SNR for planar diffuse satellite

| Symbol | Name | Units | Wavenumber-dependent? | Range | Default Value |
|-----------------|---------------------------------------|-------------------------|-----------------------|-------------------------------|---------------------------|
| A_o | area of optic | m^2 | No | | 0.1297 m^2 |
| A_{sat} | area of satellite | m^2 | No | 4 - 16 m^2 | 16 m^2 |
| $R_{sat-det}$ | distance from satellite to detector | m | No | 300 km – 1500 km | 400 km |
| $Cos(\theta_s)$ | cosine of satellite orientation angle | unitless | No | 0-1 | 0.5 |
| Δf | noise-equivalent bandwidth | Hz | No | 100-1000 Hz | 100 Hz |
| θ_{FOV} | field of view | rad | No | 25-500 mrad | 70 mrad |
| Ω_{FOV} | field of view | Sr | No | 0.63-250 mSr | 5 mSr |
| T_d | detector temperature | K | No | 77 – 300 K | 77 K |
| A_d | detector area | m^2 | No | 0.3-3.0 mm^2 | 0.5 mm^2 |
| RA | resistance-area product | $\Omega \cdot m^2$ | No | 0.133-362 $\Omega \cdot cm^2$ | 0.332 $\Omega \cdot cm^2$ |
| ν_1 | minimum wavenumber | cm^{-1} | Yes | 2000-25000 cm^{-1} | |
| ν_2 | maximum wavenumber | cm^{-1} | Yes | 2000 – 25000 cm^{-1} | |
| $\Delta \nu$ | spectral resolution | cm^{-1} | No | 1 - 5 cm^{-1} | 5 cm^{-1} |
| η | quantum efficiency | unitless | Yes | 0 - 1 | 1 |
| k_o | electronic efficiency | unitless | No | 0 – 1 | 1 |
| τ_o | transmission of optics | unitless | Yes | 0 - 1 | 1 |
| τ_f | transmission of filters | unitless | Yes | 0 - 1 | 1 |
| τ_{atm} | transmission of atmosphere | unitless | Yes | 0 - 1 | 1 |
| ρ_{sat} | reflectance of satellite | unitless | Yes | 0 - 1 | 1 |
| L_{e-back} | background radiation | W/ $cm^2 Sr cm^{-1}$ | Yes | | |

PLEXUS-determined atmospheric transmission and background radiation

The transmission of the atmosphere and the background radiance were determined using PLEXUS, an atmospheric modeling tool developed by the Air Force Research Laboratory. PLEXUS provides a graphical user interface for MODTRAN, LOWTRAN, and SAMM, (SHARC3 and MODTRAN2 Merged), which are modeling codes that produce atmospheric transmission and background radiation. PLEXUS guides the user through a series of options with defaults in place, allowing the user to change the default settings for time, date, location, and atmospheric conditions. PLEXUS may be run in novice, intermediate, or advanced mode, each mode allowing increasingly more default settings to be altered. In this model, PLEXUS was always run in novice mode.

Initially, the model was set up to detect a star of the same size and range as Vega, with the same effective temperature as the sun. From a telescope in Dayton, OH, (38.89° N, -77.01° E), at 1730 GMT and 0 m elevation, the telescope was pointed with an azimuthal angle of 70.7536° and a zenith angle of 44.7776°, which corresponded to the location of Vega at the time and date of the simulated observation. The azimuthal angle is measured from 0° to 360° from north, and the zenith angle is measured from 0° to 90° from the zenith.

PLEXUS allows the user the opportunity to vary visibility between 50 km and 0.2 km. Unless otherwise specified, the visibility was set to 23.0 km, which is a standard atmospheric model. PLEXUS also has aerosol settings for urban, rural, desert, and maritime environments. Rural aerosol settings were used for every simulation unless stated otherwise.

The atmospheric transmission and background radiation were collected over a wide wavelength band, from 0.4 μm to 12 μm , with a resolution of 5 cm^{-1} . Data was collected in three parts in order to limit the amount of data in each file and to overcome a discontinuity in PLEXUS at 1.39 μm . Wavelengths less than 1.39 μm were not included in the SAMM model, so PLEXUS was run using MODTRAN. The first set of data included atmospheric transmission and background radiation from 0.4 to 0.7 μm using MODTRAN. The second set of data included atmospheric transmission and background radiation from 0.7 to 1.39 μm , also using MODTRAN. The third set of data included atmospheric transmission and background radiation from 1.39 to 12 μm using SAMM. Atmospheric transmission was given in unitless numbers ranging from zero to one, and background radiance was given in units of power per area per solid angle per inverse centimeter. All radiometric units in the model were converted to wavenumbers in order to accommodate the data provided by PLEXUS.

Approximations

It is important to determine how each of the parameters discussed above affects the SNR so that an optimal detection system can be developed. Variables may be divided into those that are wavelength-dependent and those that are wavelength independent. Wavelength-independent parameters have a more straightforward effect on SNR because they are independent of the wavelength band.

Small Signal Noise Approximation.

Without making approximations, it is difficult to determine how the SNR depends on various parameters. In the case of daytime satellite detection, the number of photons incident on the detector from the background radiation is much greater than the number

of photons incident on the detector from the target, so the shot noise due to the signal is much smaller than the shot noise due to the background. When signal noise is much smaller than background noise, the signal noise can be approximated as zero. This approximation is valid unless the FOV is made very small. In the limit, as θ_{FOV} approaches zero, the required θ_{FOV} to invalidate this approximation for a 16 m^2 satellite at 400 km under ideal observation conditions is on the order of $100 \text{ } \mu\text{rad}$, which is too small for detecting satellites that may be off-orbit. Therefore, this approximation is valid for daytime observation conditions. The small-signal approximation is valid when signal shot noise is much less than background shot noise, which is true for daytime detection. Then, the signal shot noise may be approximated as zero.

Ignoring signal noise, then, the equation for the SNR becomes

$$SNR \approx \frac{k_o A_{sun} A_{sat} \cos(\theta_s)}{\pi R_{sun-sat}^2 R_{sat-det}^2 \sqrt{\Delta f}} \frac{\frac{q A_o}{hc} \sum_{v=v_1}^{v_2} \eta \tau_o \tau_f \tau_{atm} \rho_{sat} \frac{1}{v^3} \Delta v}{\sqrt{\frac{2 q^2 A_o}{hc} \Omega_{FOV} \sum_{v=v_1}^{v_2} \eta \tau_o \tau_f L_{e-back} \frac{1}{v^3} \Delta v + \frac{4 k T_d A_d}{RA}}} \quad (29)$$

Since PLEXUS returns discrete values for atmospheric transmission and background radiance, the integrals in Equation (17) are converted to summations across the band of interest. Now, the dependence of several scalar parameters can be approximated. These parameters and the SNR dependence on them in the daylight approximation are listed in Table 3. In the small signal limit, the SNR depends linearly on the area of the satellite and the cosine of the orientation angle. The SNR depends on the inverse of the square of the distance between the satellite and detector and depends on the inverse of the square root of the noise-equivalent bandwidth of the detector.

Table 3: Parameter list for small signal noise approximation

| Symbol | Name | Units | Default | Dependence |
|-----------------|---------------------------------------|----------------|------------------|--------------|
| A_{sat} | area of satellite | m ² | 9 m ² | linear |
| $R_{sat-det}$ | distance from satellite to detector | m | 400 km | $1/x^2$ |
| $Cos(\theta_s)$ | cosine of satellite orientation angle | unitless | 0.5 | linear |
| Δf | noise-equivalent bandwidth | Hz | 100 Hz | $1/\sqrt{x}$ |

BLIP Approximation.

Background-limited infrared photodetection (BLIP) is detection in the case that background noise dominates all other noise sources. From initial analysis, background noise is much larger than signal noise for daytime detection. When background noise is also much larger than detector noise, the BLIP approximation can be made, and the SNR can be approximated as

$$SNR \approx \frac{k_o A_{sun} A_{sat} \cos(\theta_s)}{\pi R_{sun-sat}^2 R_{sat-det}^2} \sqrt{\frac{A_o h c}{2 \Omega_{FOV} \Delta f}} \frac{\sum_{\nu=\nu_1}^{\nu_2} \eta \tau_o \tau_f \tau_{atm} \rho_{sat} \frac{1}{\nu^3} \Delta \nu}{\sqrt{\sum_{\nu=\nu_1}^{\nu_2} \eta \tau_o \tau_f L_{e-back} \frac{1}{\nu^3} \Delta \nu}} \quad (30)$$

In BLIP mode, then, the dependence of SNR on several variables becomes apparent. Variables and their effect on the SNR when the BLIP approximation is valid are listed in Table 4. When background noise dominates, the SNR depends linearly on the area of the satellite and the cosine of the orientation angle of the satellite. The SNR depends on the inverse of the square of the distance between the satellite and detector. The SNR depends on the square root of the area of the optic and depends on the inverse of the square root of both the noise-equivalent bandwidth and the solid angle FOV, Ω_{FOV} .

The FOV greatly impacts the SNR of the detection system. As shown in Equation (30), when the BLIP approximation is valid, SNR depends on the reciprocal of the square root of Ω_{FOV} . As the FOV decreases, background noise decreases and no longer dominates detector noise, so the BLIP approximation becomes invalid. Figure 11 shows a plot of the true SNR and the BLIP SNR as a function of θ_{FOV} for the band from 1.2 to 1.3 μm . All other parameters are the default parameters listed in Table 2.

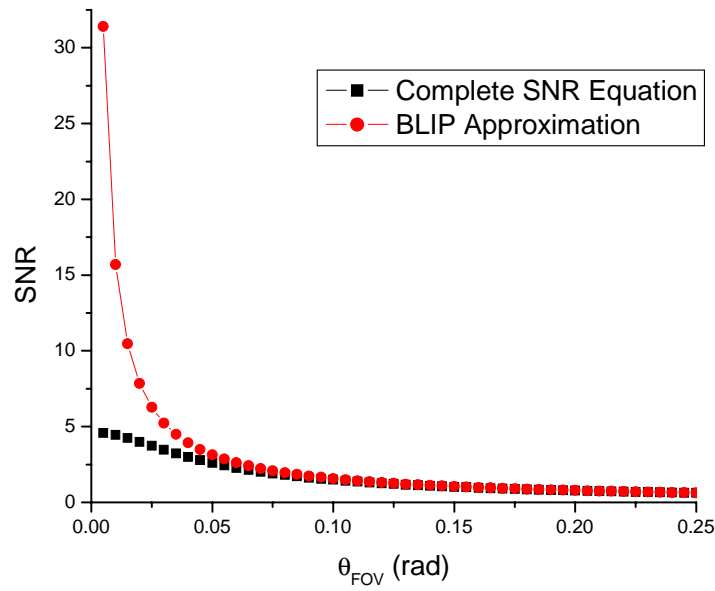


Figure 11: Comparison of SNR (black) and BLIP SNR (red) as a function of FOV from 1.2 μm to 1.3 μm

When default parameters are used for the 1.2- to 1.3- μm band, the BLIP approximation produces a SNR that deviates from the true SNR by more than 1.0% when θ_{FOV} is less than 0.24 rad. This is much larger than the θ_{FOV} used for daytime detection, so the BLIP approximation may not be used; however, the estimate that SNR depends on the reciprocal of the square root of Ω_{FOV} is a good first approximation.

These approximations are used only to simplify the SNR equation in order to determine, analytically, the dependence of the SNR on various parameters. The complete equation for SNR for a photovoltaic detector given in Equation (17), with summations instead of integrals to accommodate discrete values of atmospheric transmission and background radiation provided by PLEXUS, is used to compute all of the results discussed in Chapter IV.

Table 4: Parameter list for BLIP approximation

| Symbol | Name | Units | Default Value | Dependence |
|-----------------|-------------------------------------|----------------|-----------------------|--------------|
| A_{sat} | satellite area | m ² | 9 m ² | linear |
| $R_{sat-det}$ | distance from satellite to detector | m | 400 km | $1/x^2$ |
| $Cos(\theta_s)$ | orientation angle | unitless | 0.5 | linear |
| A_o | area of optic | m ² | 0.1297 m ² | \sqrt{x} |
| Δf | noise-equivalent bandwidth | Hz | 100 Hz | $1/\sqrt{x}$ |
| Ω_{FOV} | field of view | Sr | 0.005 Sr | $1/\sqrt{x}$ |

Parameters investigated in this research

Parameters that remain to be investigated, then, are the area of the optic, quantum efficiency, transmissions of the optics, filters, and atmosphere, background radiation, reflectance of the satellite, FOV, detector parameters, band center, and bandwidth. In order to determine how the SNR depends on these parameters, the model was exercised for various scenarios and conditions. The results and analysis of these exercises are presented in the following chapter.

IV. Analysis and Results

The goal of this research is to produce a model of a daytime satellite detection system in order to determine optimal and limiting observing conditions. Part of this process involves determining trends among the variables. In many cases, the trend is more important to this research than the magnitude of the SNR values calculated. For example, for a diffuse, planar satellite, the SNR increases as the detector is placed at higher altitudes. This is true when all other parameters are held constant, whether the other parameters are ideal or set to represent a real system. In either case, the trend reveals that, when all other parameters are held constant, the ideal observing case is when the detector is located at high altitude.

In reality, many parameters interact in complex ways, causing trends to be difficult to identify. In the above example, the location of the satellite may require a detector at high altitude to point low on the horizon in order to detect the satellite. The thicker atmosphere between the target and detector decreases the SNR. The dependence of SNR on the variables is more complicated when their interactions are considered.

The results presented here do not present trends involving interactions of variables. Instead, the purpose of this research is to present the end-to-end model and to illustrate trends for one parameter at a time, holding all other parameters constant. For example, the results presented here will not show the optimal satellite and detector locations, but will show instead that daytime satellite detection is more likely to occur when the detector is placed at high altitudes, and that detection of a planar diffuse satellite is less likely when the satellite is low on the horizon.

Specifically, the parameters investigated in this research include optimal bands for detecting reflected sunlight from a planar diffuse satellite, trends in the SNR related to the FOV, and effects of detector parameters, detector altitude, observation angle, and atmospheric conditions of daytime satellite detection. Before these parameters are investigated using the model, the model must be validated by comparing the SNR produced by the model for some daytime scenario with published results.

Validation

Daytime star detection was achieved and documented in the 1983 paper, “Ground-Based Electro-Optical Surveillance of Satellites in Daylight by Detection of Reflected Sunlight,” (Rork, 1983:106). Polaris was detected through a window with a 150-mm focal length f/5 lens on 31 December 1980. A Kodak Wrattan series No. 87 filter was used to block all wavelengths below 0.8 μm (Rork, 1983:105), with transmission coefficient equivalent to 0.27 for the signal and 0.037 for the background (Rork, 1983:106). The average quantum efficiency of the detector was found to be 0.64 (Rork, 1983:105). The noise-equivalent bandwidth, which is the reciprocal of the integration time, was 30 Hz (Rork, 1983:105). The detector used was a silicon array, with sensitivity to 1.1 μm , and θ_{FOV} was 0.23°, or 4 mrad.

Atmospheric conditions were modeled for an observer at sea level in Lincoln, MA, at latitude 42.4468° and longitude -71.2255°, (where negative longitude corresponds to west), on 31 December 1980 at 1730 GMT. Aerosols were set to those for a rural environment on a clear day with standard visibility (23.0 km). The viewing angle of the telescope was chosen by determining the elevation and azimuthal angle of Polaris at the given date and time, given that Polaris has a Right Ascension of 2:31 and a declination of 89°15’

(Stroble, 2004:6). Values used for the radius and range of Polaris were 100 AU and 360 light years, respectively (Frommert and Kronberg, 2005:1). At 1730 GMT, for an observer in at the coordinates above, the elevation was 42.246° from the horizon and the azimuthal angle was 0.977746° east of north. The algorithm used to compute elevation and azimuthal angles from Right Ascension and declination coordinates is given in Appendix B. The BLIP approximation was used for this scenario because it was a stated assumption in the Rork paper. The SNR equation used to validate the model is given in Equations (31) and (32):

$$SNR = \frac{\frac{k_o q A_o}{hc} \sum_{v=v_1}^{v_2} \eta \tau_o \tau_{f-sig} \tau_{atm} E_{e-star}^{opt} \frac{1}{v^3} \Delta v}{\sqrt{\frac{2q^2 A_o \Delta f}{hc} \Omega_{FOV} \sum_{v=v_1}^{v_2} \eta \tau_o \tau_{f-back} L_{e-back} \frac{1}{v^3} \Delta v}} \quad (31)$$

and, when the irradiance of the star is included in terms of the star area and range,

$$SNR = \frac{k_o A_{star} \cos(\theta_s)}{R_{star}^2} \sqrt{\frac{A_o}{2hc\Delta f \Omega_{FOV}}} \frac{\sum_{v=v_1}^{v_2} \eta \tau_o \tau_{f-sig} \tau_{atm} L_{e-star}(v, T_{star}) \frac{1}{v^3} \Delta v}{\sqrt{\sum_{v=v_1}^{v_2} \eta \tau_o \tau_{f-back} L_{e-back} \frac{1}{v^3} \Delta v}} \quad (32)$$

Values of parameters input into the model to determine the SNR are shown in Table 5. The summation was performed over all the wavelengths for which the detector was sensitive. The effects of the filter were included by using effective filter transmission coefficients that were wavenumber-independent and gave the total attenuation of the signal or background over all wavenumbers seen by the detector. Transmission of the

optics was approximated to be 1, since there was no data for optical transmission presented in the paper.

The SNR calculated using the daytime model was 6.91. This value is larger than the published value of 6 by a factor of 15%. If the equation were evaluated with an optical transmission coefficient of 0.75 instead of 1, the SNR predicted by the daytime model would be 6, as discussed in the paper. The daytime model predicts the SNR for the daytime star detection scenario published in the paper, so the model is valid for daytime detection.

Table 5: Values of parameters used to validate SNR model

| Variable Symbol | Value | Units |
|------------------------|----------------------|---|
| A_{star} | $1.52 \cdot 10^{16}$ | km^2 |
| R_{star} | $4.06 \cdot 10^{13}$ | km |
| A_o | 7.07 | cm^2 |
| $\text{Cos}(\theta_s)$ | 1 | unitless |
| Δf | 30 | Hz |
| θ_{FOV} | 4 | mrad |
| Ω_{FOV} | 16 | μSr |
| ν_1 | 9091 | cm^{-1} |
| ν_2 | 33333 | cm^{-1} |
| $\Delta \nu$ | 1 | cm^{-1} |
| η | 0.64 | unitless |
| τ_o | 1 | unitless |
| k_o | 1 | unitless |
| τ_{f-sig} | 0.27 | unitless |
| τ_{f-back} | 0.037 | unitless |
| T_{star} | 7000 | K |
| τ_{atm} | function of ν | unitless |
| L_{e-back} | function of ν | $\text{W}/(\text{cm}^2 \text{Srcm}^{-1})$ |

Optimal bands

Optimal bands were found by running the model for different bandwidths and band centers. The model was run for an observer at 38.89° latitude and -77.01° longitude, (where a positive number corresponds to east), at sea level, with the telescope pointing at

a zenith of 44.7776° and an azimuth of 70.7536° east of north. This viewing angle corresponded to the location of Vega for 25 October 2005, at 1730 GMT, at the location chosen. It was a useful choice because the viewing angle was not ideal. Aerosols were set to those for a rural environment on a clear day with standard visibility (23.0 km). All atmospheric data used in this analysis was taken for this date, time, location, viewing angle, aerosol, and visibility conditions unless stated otherwise. Graphs of atmospheric transmission and background radiance are shown in Figures 12 and 13.

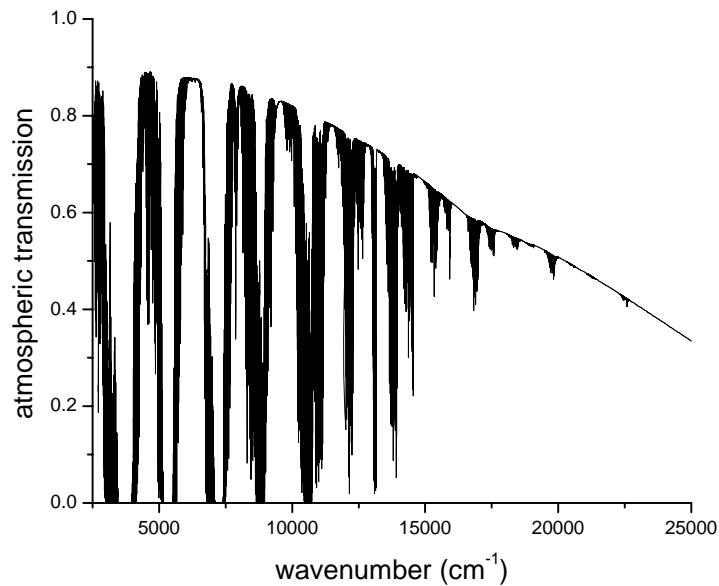


Figure 12: Atmospheric transmission from 2500 cm^{-1} to 25000 cm^{-1} ($0.4\text{ }\mu\text{m}$ to $4.0\text{ }\mu\text{m}$)

Dips in the graph of atmospheric transmission are caused by absorption of those wavelengths by different constituents of the atmosphere. Some strong absorption lines in the wavelength region between 0.4 and $12.0\text{ }\mu\text{m}$ include those of CO_2 at $2.7\text{ }\mu\text{m}$ (3660 cm^{-1}), $4.3\text{ }\mu\text{m}$ (2350 cm^{-1}), and between 11.4 and $12\text{ }\mu\text{m}$ ($833\text{--}875\text{ cm}^{-1}$), and those of water vapor at $1.38\text{ }\mu\text{m}$ (7246 cm^{-1}), $1.87\text{ }\mu\text{m}$ (5332 cm^{-1}), $2.70\text{ }\mu\text{m}$ (3700 cm^{-1}), and

6.27 μm (1595 cm^{-1}) (Wolfe and Zissis, 1989:5-70,5-73,5-82). The SNR is expected to be low in regions surrounding these absorption lines.

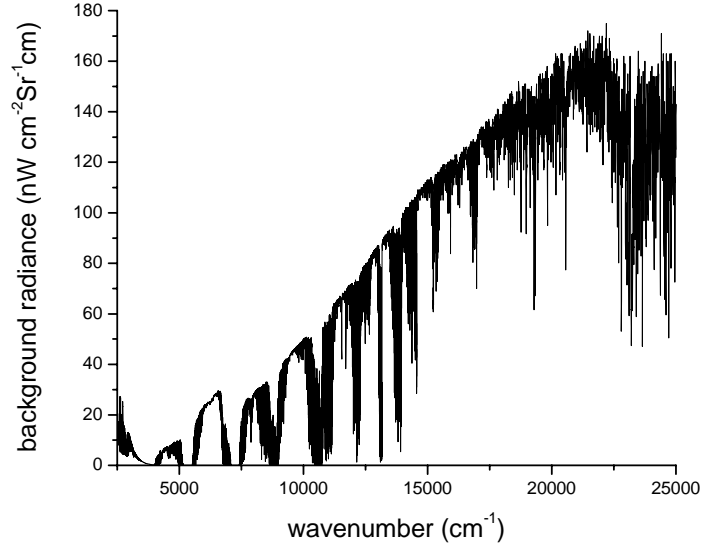


Figure 13: Background radiance from 2500 cm^{-1} to 25000 cm^{-1} ($0.4\text{ }\mu\text{m}$ to $4.0\text{ }\mu\text{m}$)

To determine ideal bands, the SNR was found for a series of 500-nm bands centered from $0.75\text{ }\mu\text{m}$ to $4.75\text{ }\mu\text{m}$, and for a series of 100-nm bands centered from $0.45\text{ }\mu\text{m}$ to $4.95\text{ }\mu\text{m}$. Default values were used for all parameters listed in Table 2 except for the minimum and maximum wavenumbers. Graphs of the resulting SNR as a function of band center are displayed in Figures 14 and 15.

The SNRs calculated for both 500-nm bandwidths and 100-nm bandwidths are largest in the near-infrared region, from 0.8 to $1.7\text{ }\mu\text{m}$. The large dip in the SNR for 100-nm bands centered at 1.35 and $1.45\text{ }\mu\text{m}$ is due to a water vapor absorption line centered at $1.38\text{ }\mu\text{m}$. It is not apparent in the 500-nm graph because the large band from 1.0 to $1.5\text{ }\mu\text{m}$ includes enough of the band outside the absorption line to compensate for the region of low transmission.

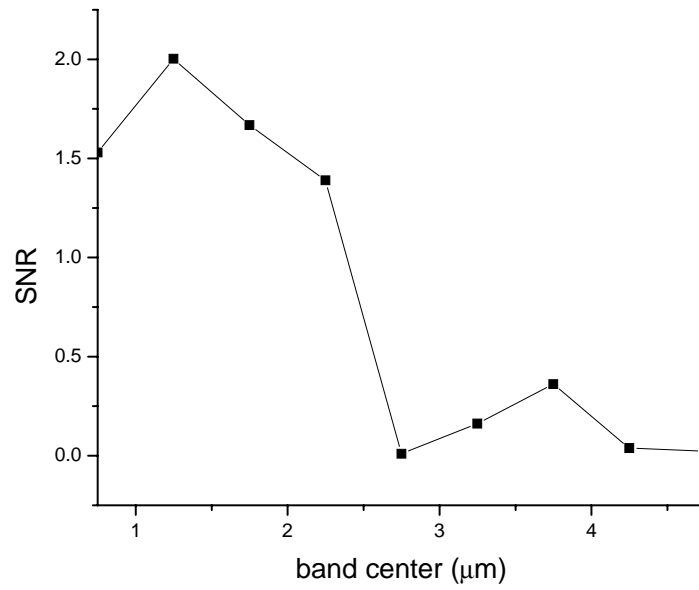


Figure 14: SNR for 500-nm bands centered from 0.75 μm to 4.75 μm

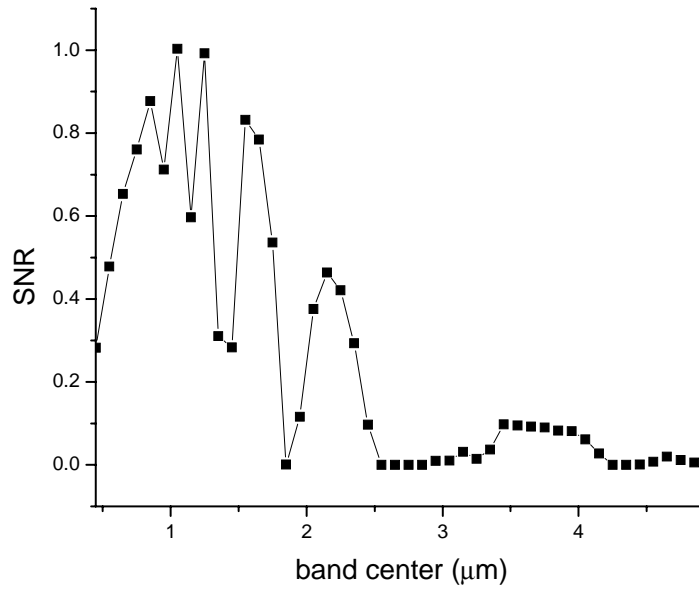


Figure 15: SNR for 100-nm bands centered from 0.45 μm to 4.95 μm

The regions of the spectrum that yield high SNRs correspond to those that simultaneously exhibit high atmospheric transmission and low background radiation.

Graphs of the atmospheric transmission and background radiation obtained from PLEXUS illustrate that when θ_{FOV} is 70 mrad, the ideal detection band is between 0.8 and 1.7 μm (5882.35 and 12500 cm^{-1}). At wavelengths less than 0.8 μm , low atmospheric transmission decreases the SNR, and at wavelengths greater than 1.8 μm , high background radiation decreases the SNR.

The magnitude of the atmospheric transmission and background radiance depend on the position of the sun, the altitude of the observer, and the angle of observation. The optimal bands depend on the content of the atmosphere during observation, which varies with weather, altitude, and environment. If reflectivity of the satellite, quantum efficiency, and transmission of the optics are treated as functions of wavenumber, the optimal bands will depend on these parameters, as well. The model is easily adapted to accommodate wavelength-dependent functions instead of scalars, and additional research may investigate optimal bands for specific satellite materials or detectors with well-known reflectivity, quantum efficiency, or transmission coefficient functions.

Field of View Survey

The optimal FOV for daytime satellite detection must satisfy two competing conditions. The FOV must be large enough to allow a satellite that is off course to cross it, but must be small enough to limit the background radiation, so that the SNR will be large enough to detect the satellite. For a satellite that is 1 km off orbit for every 100 km of altitude, θ_{FOV} must be at least 10 mrad, or the off-orbit satellite will pass outside the FOV. A θ_{FOV} of 70 mrad allows for orbital error of 7 km for every 100 km of altitude. For LEO satellites that range from 200 to 3000 km in altitude, a θ_{FOV} of 70 mrad allows orbital error from 14 km for the nearest satellites to 211 km for those furthest away.

Larger FOVs will limit the SNR more for bands in which the background radiation is higher. A comparison of the influence of FOV on SNR for three different 100-nm wide bands is shown in Figure 16. Narrowing the FOV causes the SNR to increase most rapidly for the 0.8-0.9- μm band, (11111-12500 cm^{-1}), which has the highest background radiation of the three. Similarly, the SNR increases more for decreased FOV for the 1.0-1.1- μm band, (9090-10000 cm^{-1}), than for the 1.2-1.3- μm band, (7692-8333 cm^{-1}), because there is higher contribution from the background in the 1.0- to 1.1- μm band than in the 1.2- to 1.3- μm band. This important result demonstrates that the FOV may dictate the ideal band. For a large θ_{FOV} of 50 mrad, the ideal 100-nm band is between 1.0 and 1.1 μm , but for the smaller θ_{FOV} of 5 mrad, the ideal 100-nm band is between 0.6 and 0.7 μm . The choice of θ_{FOV} determines ideal bands, which determine the best detector to use.

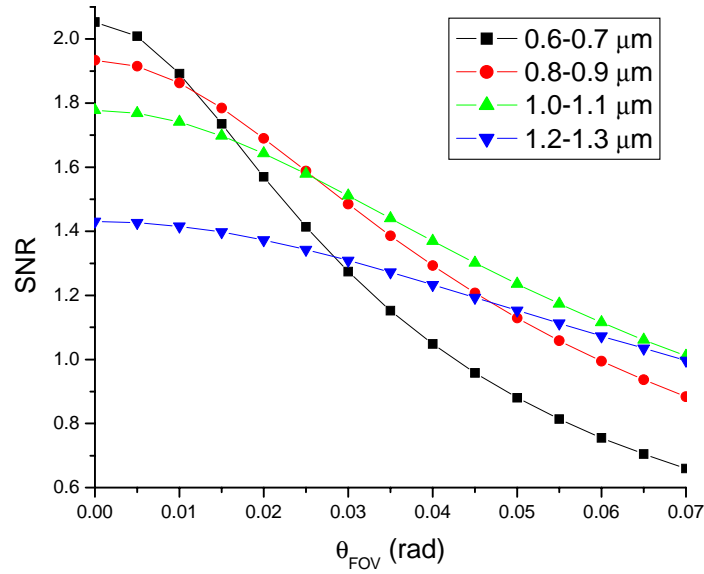


Figure 16: SNR as a function of FOV for 0.6-0.7 μm (black), 0.8-0.9 μm (red), and 1.0-1.1 μm (green), and 1.2-1.3 μm (blue) for 100-nm wide bands

Detector Survey

Once optimal bands are determined, detectors can be compared to find the detector that is sensitive across the correct wavelengths and that results in the highest SNRs. The choice of detector depends on the detection scenario. As shown in Figure 16, changes such as decreasing the FOV can cause the optimal band to shift from one region to another. This detector survey is based on a minimum θ_{FOV} of 70 mrad, which allows detection of satellites off-orbit by as much as 7 km for every 100 km of altitude. In this case, the best wavelength region for detection is between 1.0 and 1.3 μm .

Values of detector parameters for Hamamatsu InGaAs PIN photodiodes are included in Table 6 (Hamamatsu Corporation, 2005:1). The RA product was calculated using Equation (27). SNRs were calculated for the entire band over which each detector was sensitive, (shown in Table 6), as well as over the band from 1.2 to 1.3 μm , using default values listed in Table 2 for all parameters except detector area and RA product. The computation of SNR over the 100-nm band from 1.2 to 1.3 μm allows a direct comparison of the different detectors.

It is apparent from the results in Table 6 that, apart from bandwidth, dark current is the most significant parameter affecting SNR. For the test conditions, dark currents of more than 48 μA cause the SNR to drop below one. The best detector is sensitive over the bands which allow high atmospheric transmission and low background radiance, and has low dark current.

Thermal Emissions

The model presented in this research may be used to calculate the SNR when the signal irradiance is due to reflected sunlight. For very hot satellites such as nuclear-

powered satellites, for satellites in the earth's shadow that do not reflect sunlight, or for satellites tilted at such an angle that they reflect very little sunlight, thermal emissions from the satellite may dominate the signal. It is important to determine the conditions under which thermal emissions of the satellite are comparable to reflected sunlight.

Table 6: Detector parameters and SNRs for InGaAs PIN photodetectors at T = 77 K

| Name | Active Area (mm ²) | λ_{\min} (μm) | λ_{\max} (μm) | dark current (nA) | RA (Ω-cm ²) | SNR over entire band | SNR for 1.2-1.3-μm band |
|-----------|--------------------------------|-----------------------|-----------------------|-------------------|-------------------------|----------------------|-------------------------|
| G5852-103 | 0.3 | 0.9 | 2.07 | 55 | 361.798 | 3.13226 | 1.3764 |
| G5852-11 | 1 | 0.9 | 2.07 | 500 | 132.659 | 3.13055 | 1.37076 |
| G5852-13 | 3 | 0.9 | 2.07 | 5000 | 39.7978 | 3.1136 | 1.31744 |
| G8422-03 | 0.3 | 0.9 | 2.1 | 550 | 36.1798 | 3.17238 | 1.37013 |
| G8422-05 | 0.5 | 0.9 | 2.1 | 1250 | 26.5318 | 3.16971 | 1.36143 |
| G8372-01 | 1 | 0.9 | 2.1 | 5000 | 13.2659 | 3.15552 | 1.31744 |
| G8372-03 | 3 | 0.9 | 2.1 | 50000 | 3.97978 | 2.99883 | 0.992243 |
| G5853-203 | 0.3 | 1.2 | 2.55 | 1000 | 19.8989 | 3.28196 | 1.36452 |
| G5853-21 | 1 | 1.2 | 2.55 | 4000 | 16.5824 | 3.25917 | 1.32875 |
| G5853-23 | 3 | 1.2 | 2.55 | 75000 | 2.65318 | 2.82866 | 0.890911 |
| G5853-103 | 0.3 | 1.2 | 2.57 | 2000 | 33.1648 | 3.27404 | 1.35228 |
| G5853-11 | 1 | 1.2 | 2.57 | 7500 | 8.84395 | 3.23292 | 1.29038 |
| G8373-13 | 3 | 1.2 | 2.57 | 150000 | 1.32659 | 2.51938 | 0.708444 |
| G8373-01 | 1 | 1.2 | 2.6 | 75000 | 0.884395 | 2.82815 | 0.890911 |
| G8373-03 | 3 | 1.2 | 2.6 | 1500000 | 0.132659 | 1.15959 | 0.256674 |
| G8423-03 | 0.3 | 1.2 | 2.6 | 20000 | 0.994944 | 3.1443 | 1.17633 |
| G8423-05 | 0.5 | 1.2 | 2.6 | 50000 | 0.663296 | 2.95953 | 0.992243 |

For a satellite without a major heat source on board, thermal emission is primarily due to reflection of the earth's inherent thermal radiation (Grishin, 1999:5). Radiance produced by a blackbody at 300 K peaks at 9.66 μm, and in the 0.4- to 5.0-μm region, the orientation angle of the satellite would have to be within 10 nrad of $\pi/2$ in order for thermal emission from a 300-K blackbody to overcome the radiance due to reflected sunlight. For most orientations, then, radiance due to reflected sunlight is greater than radiance due to reflection of the earth's thermal radiation.

If the satellite is completely in the earth's shadow, then the model can be adapted by replacing the signal irradiance term in the numerator and denominator of the SNR equation (E_{e-sig}^{opt}) with the blackbody exitance equation for $T = 300$ K. The ideal bands shift toward longer wavelength IR because the peak wavelength of the signal irradiance shifts to $9.66 \mu\text{m}$. Detectors must also be changed to those sensitive at longer wavelengths.

Satellites with an on-board heat source, such as nuclear-powered satellites, must only be hot enough for their inherent thermal emission to overcome reflected sunlight. A comparison between the inherent thermal radiation of satellites of 500 K and 600 K in the band from $0.4 \mu\text{m}$ to $5.0 \mu\text{m}$ is shown in Figure 17. Radiance of the reflected sunlight is calculated using the solar spectrum described in the previous chapter, the orientation angle $\theta_s = 45^\circ$, and an ideal reflectivity of $\rho = 1$. Across the band from $0.4 \mu\text{m}$ to $5.0 \mu\text{m}$, the blackbody must reach a temperature of $T = 533$ K to overtake the radiance produced by reflected sunlight. Thermal emission of satellites must be considered if the satellite has an on-board heat source that causes it to reach temperatures greater than 500 K, or if detection occurs at wavelengths greater than $3.0 \mu\text{m}$.

Visibility Survey

Visibility has a strong effect on SNR. As expected, low visibility produces low SNRs. All of the simulations so far have assumed a standard visibility of 23.0 km. PLEXUS allows the user to vary the visibility between 50 km and 200 m. Atmospheric transmission decreases strongly with decreased visibility. Figure 18 includes a graph of atmospheric transmission for various visibility levels. For visibility less than 5.0 km, the

atmospheric transmission across the spectrum from $0.4\ \mu\text{m}$ to $12.0\ \mu\text{m}$ ($833\ \text{cm}^{-1}$ to $25000\ \text{cm}^{-1}$) is less than 0.2 and daytime detection is impossible.

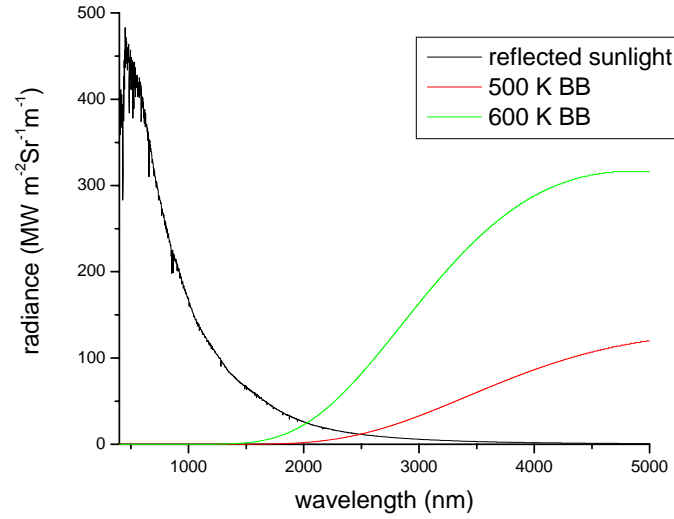


Figure 17: Radiance of reflected sunlight (black) and blackbodies of 500 K (red) and 600 K (green)

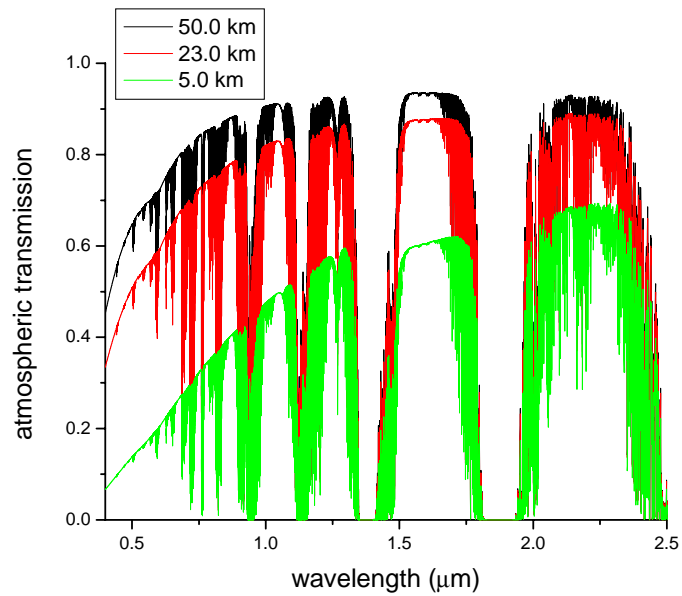


Figure 18: Atmospheric transmission for different visibility levels: 50.0 km (black), 23.0 km (red), 5.0 km (green)

SNR decreases with decreased visibility. Although visibility as high as 50 km is not necessary for daytime detection, higher visibility produces better results. A graph of SNRs over 100-nm bands centered from 0.55 μm to 2.45 μm is shown in Figure 19. All parameters other than visibility are the default parameters listed in Table 2. The decrease in SNR as visibility is lowered corresponds to the smaller atmospheric transmission at lower visibilities. For visibility of 50.0 km, the SNR is greater than one for 100-nm bands centered at 0.65, 0.75, 0.85, 1.05, 1.25, and 1.55 μm . When the visibility drops to 23.0 km, only the 100-nm band centered at 1.05 μm is greater than one. When the visibility is only 5.0 km, there are no 100-nm bands that produce SNRs greater than one. In order to achieve daytime detection in low visibility, then, other parameters must be optimized to achieve detection distinct from noise.

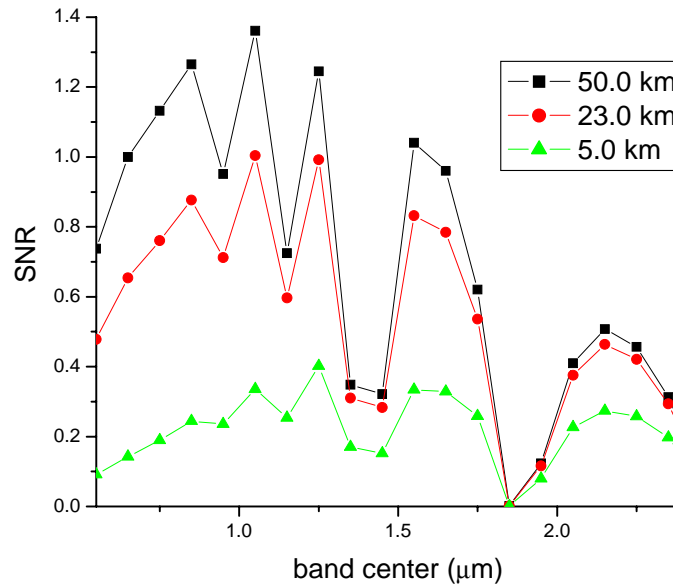


Figure 19: SNRs for 100-nm bands centered from 0.55 μm to 2.45 μm for visibilities of 50.0 km (black), 23.0 km (red), 5.0 km (green)

Aerosol Survey

When run in novice mode, PLEXUS allows the user to set the aerosol content of the atmosphere to simulate urban, rural, desert, or maritime environments. Environment impacts atmospheric transmission and background radiation because greater density of different types of particles cause absorption lines to broaden and causes increased scattering. SNRs over 100-nm wide bands centered from 0.55 μm to 2.45 μm were calculated for all four different environments and compared. A graph showing the SNRs of the different aerosol environments is shown in Figure 20.

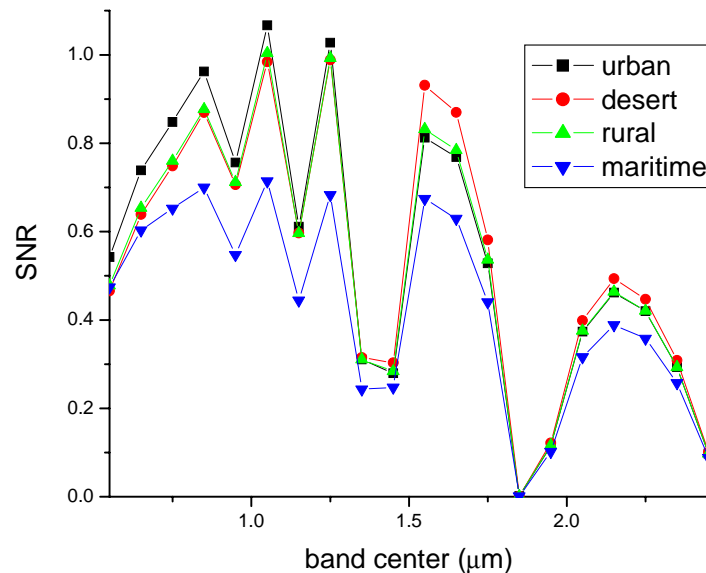


Figure 20: SNRs over 100-nm bands centered from 0.55 μm to 2.45 μm for different aerosol environments: rural (green), urban (black), desert (red), maritime (blue)

The sizes and types of particles in the atmosphere change the way light from the sun is scattered, contributing to strong daytime background radiation. If the ratio of the radius of a particle to the wavelength of light passing through it is less than 0.8, Rayleigh scattering dominates. For ratios between 0.8 and 3.0, Mie scattering occurs, and for ratios

larger than 3.0, geometric optics is sufficient to explain scattering (Wolfe and Zissis, 1989:3-70).

Types of particles contribute to background radiance and atmospheric transmittance because different materials absorb at different wavelengths. As the density of different types of particles increases, the absorption bands for that material broaden and decrease the signal in that band. In a maritime environment, for example, the amount of water vapor in the air is increased, which causes the absorption bands for water vapor to broaden and decrease the SNR more in the wavelength regions surrounding water vapor absorption bands.

Altitude Survey

Atmospheric transmission and path radiance are both due to scattering and absorption caused by different materials in the atmosphere. Attenuation is greater as the signal travels through more atmosphere, so the SNR is decreased. Path radiance is also greater as more atmosphere contributes to the background, further decreasing the SNR. Graphs of SNR for 100-nm bands centered from 0.55 μm to 2.45 μm for altitudes from 0 km to 3 km are shown in Figure 21. An altitude increase from 0 km above sea level to 3 km above sea level (approximately 9850 ft), provides an average SNR increase of 74% over 100-nm bands centered between 0.55 and 2.45 μm . Simply elevating the detector to 1 km above sea level (3280 ft) increases the SNR an average of 26% above that at sea level over 100-nm bands in the same wavelength range. It may not be feasible to place all daylight sensors at such great heights, but it is worth noting that the altitude greatly enhances the SNR.

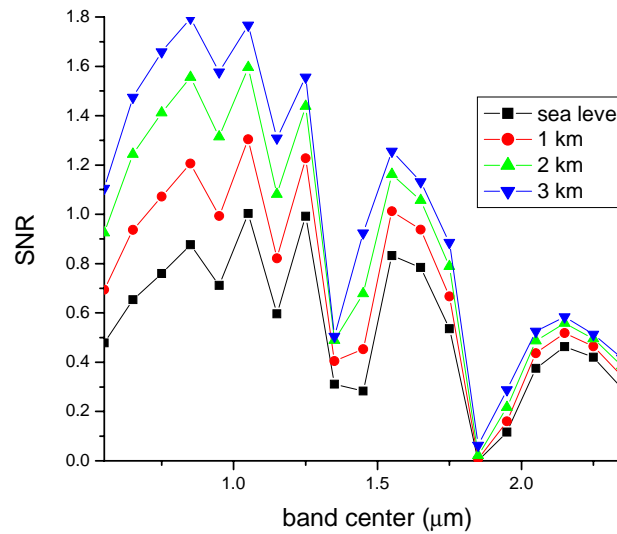


Figure 21: SNRs for 100-nm bands centered from 0.55 μm to 2.45 μm for altitudes of 0 km (black), 1 km (red), 2 km (green), and 3 km (blue)

Observation Angle Survey

As described above, atmospheric transmission and path radiance decrease as atmosphere between the target and detector increases. It may be expected that the SNR will decrease as the detector is pointed closer to the horizon, since signals from targets low on the horizon travel through more atmosphere, but an additional factor must be included when comparing SNRs for different viewing angles. The position of the sun causes the sky near the sun to be brighter, and as the detector is pointed further away from the sun, the background radiance decreases. These competing effects of decreasing atmospheric transmission and decreasing background radiance cause there to be some optimal viewing angle for a given sun location. Figures 22 and 23 include a comparison of atmospheric transmission for observation angles of 30°, 60°, and 90° from the horizon and a comparison of background radiance for observation angles of 30°, 60°, and 90° from the horizon, respectively.

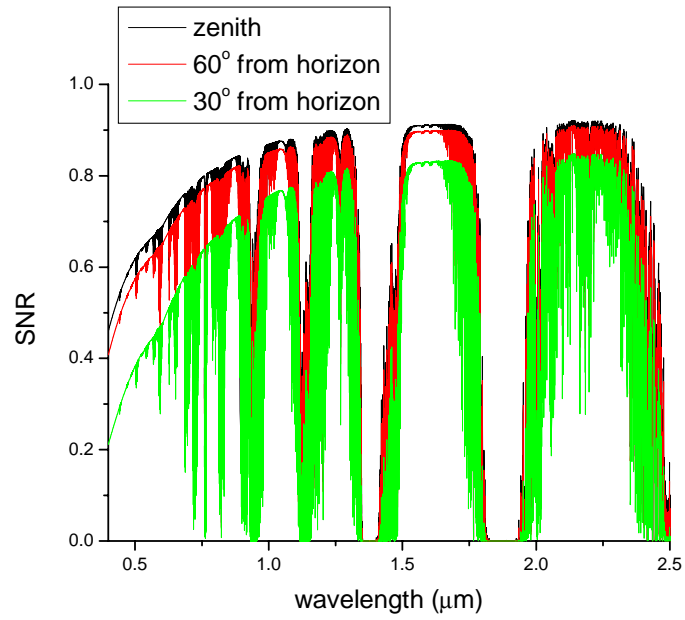


Figure 22: Atmospheric transmission for detector pointed 30° (green), 60° (red), and 90° (black) from horizon for the sun with zenith angle 51.93° and azimuth -168.46°

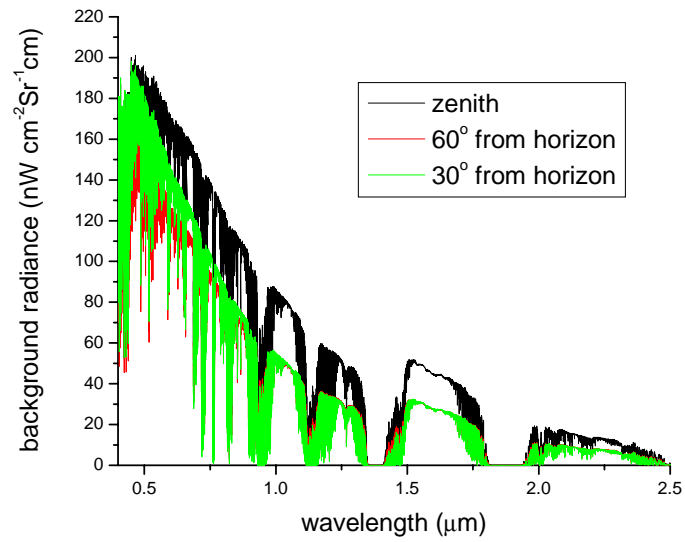


Figure 23: Background radiance for detector pointed 30° (green), 60° (red), and 90° (black) from horizon for the sun with zenith angle 51.93° and azimuth -168.46°

For the atmospheric data generated by PLEXUS for 1730 GMT on 25 October 2005, the sun is located with an azimuth of -168.46° and a zenith of 51.93° with respect to the observer. For a fixed observation azimuth of 70.75° , as the detector is swept toward the horizon, the SNR first increases due to decreasing background radiation for the dimmer sky and then increases as the thicker atmosphere attenuates the signal. A graph of SNR for observation angles 90° , 60° , and 30° from the horizon is shown in Figure 24. All other parameters are default parameters listed in Table 2.

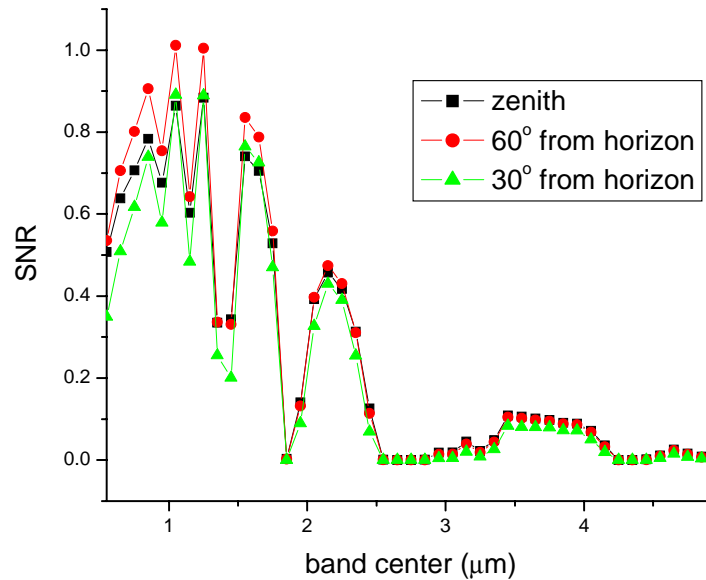


Figure 24: SNRs for 100-nm bands centered from $0.8\ \mu\text{m}$ to $1.7\ \mu\text{m}$ for detector pointed at 30° (green), 60° (red), and 90° (black) from horizon for the sun with zenith angle 51.93° and azimuth -168.46°

The SNR over 100-nm bands centered between 0.55 and $2.45\ \mu\text{m}$ increases an average of 4.0% as the detector is moved from zenith to 60° from the horizon, decreases an average of 24.1% as the detector is moved from 60° to 30° , and decreases by an

average of 99.9% as the detector is moved from 30° to the horizon. For 100-nm wide bands centered between $0.55\ \mu\text{m}$ and $2.45\ \mu\text{m}$, the largest SNRs are found when the detector is pointed 60° from the horizon, and the competing effects of decreased atmospheric transmission and decreased background radiance are balanced. The lowest SNRs are found when the detector is pointed 30° from the horizon. Intermediate values are found when the detector is pointed at the zenith.

The major conclusion to draw from this analysis is that the optimal viewing angle depends on the location of the sun in addition to the thickness of the atmosphere. In a real scenario, the viewing angle will be driven more by the location of the satellite than an attempt to optimize the SNR. A general rule for successful daylight satellite detection may be to attempt to observe satellites no closer than 30° to the horizon, and no closer than 15° from the sun.

Limits on Angular Extent of the Satellite

In the previous sections, it has been shown that atmospheric effects such as aerosol content, visibility, and atmospheric thickness can all decrease the SNR significantly. Under such conditions, the limit of the angular size of detectable objects increases and smaller satellites may travel undetected. The ratio of satellite area to the square of the distance between the satellite and detector is considered as a single parameter called the angular extent of the satellite. As shown in Table 3, SNR depends linearly on the angular extent of the satellite when daytime detection is considered. The value used for the angular extent of the satellite in the atmospheric comparisons above and throughout this paper is 100 nSr. This corresponds to a square satellite that is 4 m on a side at a distance of 400 km, or a satellite that is 8 m on a side at a distance of 800 km. When the seeing

conditions, such as visibility, altitude, or aerosol content, are not ideal, satellites that are smaller or further away may not be seen. If daylight detection of small or distant satellites is required, then the seeing conditions must be optimized to allow detection of smaller objects.

For the non-ideal case where visibility is 23.0 km, altitude is at sea level, and aerosol content is for that of a rural environment, the smallest angular extent that still produces an SNR of at least one over a 100-nm band is 0.099 nSr when θ_{FOV} is 70 mrad. This corresponds to a satellite that is 15.9 m² at 400 km, or a satellite that is 897 m² at 3000 km. On the other hand, when visibility is 50.0 km, aerosol content matches that of a desert environment, and the detector is placed at an altitude of 10,000 feet, the smallest satellite detected over a 100-nm band has an angular extent of 0.053 nSr, which corresponds to a satellite that is 8.4 m² at a 400-km range, or 475 m² at an 3000-km range. For small or distant satellites, additional techniques must be developed to increase the SNR.

Summary

In this chapter, the model was adapted to a daylight star detection scenario and validated using published data. Thermal emissions were investigated and found to be important when satellites have temperatures greater than 500 K or when detection occurs at wavelengths longer than 3.0 μm . Ideal bands were found to be between 0.8 and 1.7 μm for the default parameters chosen, and the dependence of the SNR on FOV was investigated. It was found that ideal bands depend strongly on FOV. Photovoltaic detectors that operate in the 0.8 to 1.7 μm were compared.

Dependence of SNR on different atmospheric conditions was considered. SNR was found to increase with increased visibility, decreased aerosol content, and increased altitude. The ideal observation angle was found to depend both on the thickness of atmosphere between the target and detector and the brightness of the sky. Minimum satellite sizes were calculated for ideal and non-ideal detection scenarios.

Conclusions and recommendations for areas of future research will be discussed in the next chapter.

V. Conclusions

The purpose of this research was to develop a SNR model of daytime satellite detection of reflected sunlight with a PV detector, in order to allow different detection systems to be compared and parameters to be optimized. The model incorporates daylight atmospheric transmission and background data, and includes detection noise as well as background noise in order to provide analysis of existing or proposed systems.

The product of this research is a SNR equation that models the transfer of flux from the sun to a diffuse, planar satellite to a detector on the earth in daylight conditions. The model includes satellite parameters, detector parameters, and atmospheric parameters. The model was used to determine ideal detection bands for a detection scenario, to determine which parameters have the greatest effect on SNR, and to compare various detectors and detecting conditions, as well as to determine ideal and limiting detecting conditions.

Using the Model to Analyze and Optimize Detection Systems

The SNR model used to simulate daytime detection of satellites allows the many parameters involved to be analyzed and optimized. The small signal approximation, in which the shot noise due to the signal is approximated to be zero because the background shot noise is much greater than the signal shot noise, is shown to be valid for daytime detection conditions. This can be used to simplify the SNR equation to better determine how the SNR depends on input variables such as satellite size, satellite range, and FOV. The BLIP approximation, in which background shot noise is the only noise source because it is much larger than all other noise sources, is shown to be invalid for the

InGaAs PV detector used to evaluate the model in this research. Approximations were used to analyze the SNR equation for dependence on variables, but were not used in any calculations. The SNR model can be used in the following way to design a daytime detection system.

First, the mission requirements must set the initial parameters, which include the size of the telescope used, the minimum FOV required, and the poorest atmospheric conditions under which the system must run successfully. Telescope choice determines the area of the optic, as well as the transmission of the optics. The minimum FOV is determined by the ratio of allowed orbit error to satellite range. Atmospheric conditions determine atmospheric transmission and background radiance, which can be found as functions of wavelength using atmospheric modeling tools such as PLEXUS.

Once this is accomplished, the model can be run for different spectral bands, using ideal values for the remaining parameters in order to determine the best bands for the detection scenario. Once the ideal bands are known, detectors can be chosen that are sensitive in that band and that produce little noise. The cooling system for the detector will be determined both by the band in which the detector must operate and the cost limits placed on the system.

The model can then be run again to analyze the system design or compare to existing system designs with specific detector parameters included. These simulations, which include all system parameters, can be used to determine how successful the system will be at detecting satellites in the daytime.

Recommendations for Future Research

The analysis presented in this research was limited to daytime detection with a PV detector. The model can be expanded to include noise terms due to PC detectors and thermal detectors. These noise terms were discussed in the background chapter, but not included in the analysis. Including these terms in the model would allow different types of detectors to be compared in order to optimize detection.

Ideal bands discussed in this research were for a detection system with a large θ_{FOV} of 70 mrad, used for daytime detection only. Additional research may apply the model to a dual system, designed to detect satellites both during the night and day. The model could be used to determine the FOV and optimal bands necessary for a dual system, and then to compare different detectors available in the bands determined to be best for a dual system.

In order to successfully compare the model to a real detection system, some additional considerations may be made. The model presented in this research ignores or simplifies several aspects of satellite detection that should be considered before detection systems are built and operated. These can be categorized in three groups: satellite parameters, detection parameters, and SNR improvement.

Satellite Parameters.

The model developed here is for a planar diffuse satellite whose normal vector always points toward the detector. Additional research should be done to model more realistic satellite geometries, including satellite shapes as well as orientations with respect to the detector on earth.

Additional research can focus on more accurate reflectance of satellite materials.

First, the reflectance used in this model was approximated to be independent of optical frequency. The model can be easily adapted to include reflectance as a function of optical frequency. Also, the diffuse approximation is not valid for all satellite materials. BRDFs can be used to determine reflectance coefficients of materials that are dependent on both spatial and spectral coordinates. The model can be adapted to include reflectance coefficients for materials that are partially diffuse and partially specular.

Detection Parameters.

Quantum efficiency and the transmission coefficients of the optics and filters were approximated to be wavelength-independent constants of one. More realistic values for these parameters, including wavelength-dependent functions, should be included to increase the fidelity of the model.

The SNR equation developed and used in this research models a detection system with a single-pixel detector, which limits the usefulness of the detector to simply verifying that a satellite exists in a certain location in the sky at a specific time. A more useful detection system may image the satellite in order to collect more information about it. This model can be expanded to model an imaging system with a focal plane array detector instead of a single-pixel detector. In the case of the array detector, a modulation transfer function (MTF) should be included. For a non-ideal MTF, the depth of modulation is less than one and the SNR will decrease. Physically, this is due to blurring between pixels in the detector.

Atmospheric turbulence is another parameter that was ignored in this analysis, but must be considered when designing an imaging system. Atmospheric turbulence is

caused by time-dependent temperature gradients in the atmosphere that cause refractive index gradients. These different indices of refraction induce phase changes across the signal, so the resulting image is blurred. The effect of atmospheric turbulence on daytime satellite detection and ways to minimize it should be investigated.

Atmospheric effects should be analyzed to determine the limiting conditions for which daytime satellite detection is possible. Parameters such as humidity and aerosol content contribute to atmospheric transmission and background radiance at the different altitudes, detection angles, and visibilities analyzed in this research. Further analysis of atmospheric effects and atmospheric uncertainty will determine the worst atmospheric conditions under which daytime detection can still be achieved.

SNR Improvement.

Finally, techniques to improve SNRs for daylight satellite detection should be investigated and added to the model. These techniques may include adding polarization filters to the detection system in order to attenuate the background without blocking the signal. Implementing polarization filters is difficult because the filter must be rotated in order to maintain the correct angle as the satellite travels across the sky. A model that includes the effects of polarization filters will allow the benefits of such filters to be examined. The effects of signal processing techniques can also be added to the model to determine how the SNR can be boosted by these techniques. The model can also be used to determine optimal bandwidths for various detection scenarios.

Final Conclusions.

Adapting the model to include parameters and effects such as satellite geometry, specular reflectance, atmospheric turbulence, focal plane array detectors, polarizing

filters, and signal processing techniques will allow the model to be used to more accurately describe detection systems and to design better systems for detecting satellites in the daytime.

The ability to detect satellites in the daytime will allow more frequent updates of orbital information and provide more accurate tracking of space objects. Relatively small, inexpensive daytime satellite detection systems will relieve some of the burden placed on larger, more expensive tracking radars as the number of space objects increases. A high-fidelity, end-to-end radiometric model of the daytime detection scenario allows detection systems and observing conditions to be optimized in order to design small, inexpensive daytime satellite detection systems.

Appendix A. *Mathematica* Code for Daytime Satellite Detection Model

PLEXUS runs from $1.3986\text{ }\mu\text{m}$ to $12\text{ }\mu\text{m}$, which is from 833.333 cm^{-1} to 7150 cm^{-1} , from $0.7\text{ }\mu\text{m}$ to $1.39\text{ }\mu\text{m}$, which is from 7194 cm^{-1} to 14825 cm^{-1} , and from $0.4\text{ }\mu\text{m}$ to $0.7\text{ }\mu\text{m}$, which is from 14286 cm^{-1} to 25000 cm^{-1} .

Input PLEXUS data for atmospheric transmission and background radiation

```
numpts1 = 7150-833;

filename1 = StringJoin[{"C:\PLEXUS\data_out\adi\25oct1730001"}];

trnfile1=OpenRead[StringJoin[{filename1},{".trn"}]];

trans1=Table[Read[trnfile1,{Number,Number}],{numpts1}];

Close[trnfile1];

spcfile1 = OpenRead[StringJoin[{filename1},{".spc"}]];

backrad1=Table[Read[spcfile1,{Number,Number}],{numpts1}];

Close[spcfile1];

numpts2 =14285-7194;

filename2 = StringJoin[{"C:\PLEXUS\data_out\adi\25oct1730006"}]

C:\PLEXUS\data_out\adi\25oct1730006

trnfile2=OpenRead[StringJoin[{filename2},{".trn"}]];

trans2=Table[Read[trnfile2,{Number,Number}],{numpts2}];

Close[trnfile2];

spcfile2 = OpenRead[StringJoin[{filename2},{".spc"}]];

backrad2=Table[Read[spcfile2,{Number,Number}],{numpts2}];

Close[spcfile2];

numpts3 =25000-14285+1;

filename3 = StringJoin[{"C:\PLEXUS\data_out\adi\25oct1730004"}]
```

```

C:\PLEXUS\data_out\adi\25oct1730004

trnfile3=OpenRead[StringJoin[{filename3},{".trn"}]];

trans3=Table[Read[trnfile3,{Number,Number}],{numpts3}];

Close[trnfile3];

spcfile3 = OpenRead[StringJoin[{filename3},{".spc"}]];

backrad3=Table[Read[spcfile3,{Number,Number}],{numpts3}];

Close[spcfile3];

trans=Join[trans1,trans2,trans3];

Export["C:\Documents and Settings\Katie\My
Documents\Thesis\Transdata.csv",trans];

backrad=Join[backrad1,backrad2,backrad3];

Export["C:\Documents and Settings\Katie\My
Documents\Thesis\Backraddata.csv",backrad];

 $\tau_{\text{atm}}$ =Interpolation[trans]

InterpolatingFunction[{{830.,25000.}},<>]

Lback = Interpolation[backrad]

InterpolatingFunction[{{830.,25000.}},<>]

solspec = Import["C:/Documents and Settings/Katie/My
Documents/Thesis/specwn.csv"];

solLe = Interpolation[solspec]

InterpolatingFunction[{{2000.,25000.}},<>]

(* Physical Constants *)

 $h = 6.63 \times 10^{-34}$ ; (* Js *)

```

$$\hbar = \frac{h}{2\pi} ; (* Js *)$$

$$c = 3 * 10^8 ; (* \frac{m}{s} *)$$

$$k = 1.38 * 10^{-23} ; (* \frac{J}{K} *)$$

$$q = 1.602 * 10^{-19} ; (* C *)$$

$$solrad = 6.96 * 10^8 ; (* m *)$$

$$au = 1.50 * 10^{11} ; (* m *)$$

$$ly = 9.46 * 10^{15} ; (* m *)$$

(* User Inputs - Target Parameters*)

$$Asun = \pi * (solrad)^2 ; (* area of the sun, m^2 *)$$

$$Asat = 4^2 ; (* area of the satellite, m^2 *)$$

$$Rsunsat = au ; (* distance from source to detector, m *)$$

$$Rsatdet = 400 * 10^3 ; (* distance from satellite to detector, m *)$$

(* User Inputs - Detector Parameters *)

$$ko = 1 ; (* efficiency parameter, unitless *)$$

$$\tau f = 1 ; (* filter transmission, unitless *)$$

$$res = 1 ; (* detector resolution, cm^{-1} *)$$

$$Tdet = 77 ; (* detector temperature, K *)$$

$$Df = 100 ; (* electronic bandwidth, Hz *)$$

$$B=0 ; (* 1/f noise parameter *)$$

$$\Pi=0 ; (* current for 1/f noise *)$$

$$fcutoff = 50 * 10^6 ; (* cutoff frequency, Hz *)$$

$i_{\text{dark}} = 50000 * 10^{-9}$; (* dark current, Amperes *)

$A_d = (.0005)^2$; (* detector area, m² *)

$RA = \frac{k * T_{\text{det}} * A_d}{q * i_{\text{dark}}}$; (* resistance–area product, $\Omega \text{ m}^2$ *)

(* User Inputs - Optics Parameters *)

$A_{\text{optic16}} = \pi * \left(\frac{16 * \frac{2.54}{100}}{2} \right)^2$ (* area of optic, m² *)

0.129717

(* Calculations *)

$\text{SNR}[T_{\text{det}}, A_o, \text{satangle}, \theta_s, \text{FOV}, \tau_o, \tau_f, D_f, \eta, \rho, v_1, v_2] :=$
 $k_o * A_o *$

$\text{Sum} \left[\eta * \tau_{\text{atm}}[v] * \tau_o * \tau_f * \frac{\rho * \text{solLe}[v] * A_{\text{sun}} * \text{satangle} * \text{Cos}[\theta_s]}{\pi * R_{\text{sunsat}}^2} * \right.$

$\left. \frac{1}{v^3} * \left(\frac{1}{100} \right)^3 * 100 * \text{res}, \{v, v_1, v_2\} \right] /$

$\left(h * c * \right.$

$\left. \sqrt{\left(\frac{2 * A_o * D_f}{h * c} * \right. \right.$

$\left. \left(\text{Sum} \left[\eta * \tau_{\text{atm}}[v] * \tau_o * \tau_f * \right. \right. \right.$

$\left. \left(\rho * \text{solLe}[v] * A_{\text{sun}} * \text{satangle} * \text{Cos}[\theta_s] \right) / \right.$

$\left. \left(\pi * R_{\text{sunsat}}^2 \right) * \frac{1}{v^3 * 100^3} * \text{res} * 100, \{v, v_1, v_2\} \right] +$

$\text{Sum} \left[100^2 * \text{FOV} * \tau_o * \tau_f * L_{\text{back}}[v] * \eta * \frac{1}{v * 100} * \text{res}, \right.$

$\left. \left. \{v, v_1, v_2\} \right] \right) + \frac{4 * k * T_{\text{det}} * D_f * A_d}{q^2 * RA} + \frac{B * \Pi^2}{q^4 * f} \Bigg)$

Appendix B. *Mathematica* Code for Determining Azimuth and Elevation

Determine azimuth and altitude given RA, declination, GMT, and position (latitude and longitude)

```
RAhour =2;  
RAmin =31;  
RAsec = 0;  
declindeg =89;  
declinmin =15;  
declinsec =0;  
locallatdeg = 42.4468;  
locallatmin = 0;  
locallatsec = 0;  
locallongdeg = -71.2255;  
locallongmin =0;  
locallongsec = 0;  
year = 1980;  
month = 12;  
day = 31;  
hour =17;  
minute = 30;  
second = 0;  
  
(* Compute Julian Date - from Norton's 2000.0 *)
```


If[month>2,month=month-3,If[month≤ 2,{month=month+9; year = year-1},newmonth=0]];

JD = 1721103.5+Round[365.25*year]+Round[30.6*month+.5]+day;

(* Compute Greenwich Sidereal Time *)

UT = N[hour+minute/60+second/3600] ;(* decimal hours *)

T = (JD-2451545)/36525;

T0 = 6.697374558 + (2400.051336 * T) + (0.000025862 * T²) +
(UT * 1.0027379093);

GSTdec = Mod[T0,24]; (* decimal hours *)

(* Determine Local Sidereal Time *)

long = N[locallongdeg+locallongmin/60+locallongsec/3600] ;(* decimal degrees *)

longhour = long/15; (* decimal hours *)

lat = N[locallatdeg+locallatmin/60+locallatsec/3600] ;(* decimal degrees *)

RA = RAhour+RAmin/60+RAsec/3600; (* decimal hours *)

declin =N[declindeg+declinmin/60+declinsec/3600] ;(* decimal degrees *)

LST = Mod[GSTdec+longhour,24] ;(* decimal hours *)

H = LST-RA ;(* decimal hours *)

Hangle = H*15; (* decimal degrees *)

el =

$$\text{ArcSin}\left[\cos\left[Hangle * \frac{\pi}{180}\right] * \cos\left[lat * \frac{\pi}{180}\right] * \cos\left[declin * \frac{\pi}{180}\right] + \right. \\ \left. \sin\left[lat * \frac{\pi}{180}\right] * \sin\left[declin * \frac{\pi}{180}\right]\right] * \frac{180}{\pi} \quad (* \text{ decimal degrees } *)$$

42.246

az =

$$\text{ArcTan}\left[-\left(\text{Cos}\left[\text{declin} * \frac{\pi}{180}\right] * \text{Sin}\left[\text{Hangle} * \frac{\pi}{180}\right]\right) / \right. \\ \left. \left(\text{Cos}\left[\text{lat} * \frac{\pi}{180}\right] * \text{Sin}\left[\text{declin} * \frac{\pi}{180}\right] - \right. \right. \\ \left. \left. \text{Sin}\left[\text{lat} * \frac{\pi}{180}\right] * \text{Cos}\left[\text{declin} * \frac{\pi}{180}\right] * \right. \right. \\ \left. \left. \text{Cos}\left[\text{Hangle} * \frac{\pi}{180}\right]\right)\right] * \frac{180}{\pi} (* \text{ decimal degrees } *)$$

0.977746

Bibliography

- Bondar', S. F., and others. "Estimating the possibility of observing satellites by passive optical means in twilight and daylight." *Journal of Optical Technology*. Vol. 61, No. 3: 238-242 (March 1994).
- Dereniak, Eustace L., and G. D. Boreman. *Infrared Detectors and Systems*. New York: John Wiley & Sons, Inc, 1996.
- Frommert, H., and K. Kronberg. *Polaris, Alpha Ursae Minoris*.
<http://www.seds.org/~spider/spider/Misc/alphaUMi.html> (2005). Accessed 17 Feb 06.
- Funge, Alistaire. D. *Daytime Detection of Space Objects*. MS Thesis, AFIT/GAP/ENG/05-01. School of Engineering and Management, Air Force Institute of Technology (AU), Wright-Patterson AFB, OH, March 2005.
- Grishin, E. A., and others. "Modern State of Ground-Based IR Systems for Surveying Space Objects." *Instruments and Experimental Techniques*. Vol. 42, No. 1: 1-14 (1999).
- Hall, F. F. and C. V. Stanley, "Infrared Satellite Radiometry." *Applied Optics*. Vol. 1, No. 2: 97-104 (1962).
- Hamamatsu Corporation. *InGaAs PIN Photodiodes*.
<http://sales.hamamatsu.com/en/products/solid-state-division/ingaas-pin-photodiodes/catalog.php>. (2005) Accessed 21 Nov 05.
- Marsden, J. E., and A. J. Tromba. *Vector Calculus, 4th Ed*. New York: W. H. Freeman and Company, 1996.
- Meade General Catalogue, http://www.meade.com/lx200gps/16_lx200gps.html, (2004) Accessed 22 Dec 05.
- Optics Planet, <http://www.opticsplanet.net/meade-16-lx200gps-telescopes.html>, (2005) Accessed 21 Dec 05.
- Richter, Rudolf, and Jochen Fries. "Radiometric Analysis of Infrared Sensor Performance." *Applied Optics*. Vol. 27, No. 22: 4771-4776. (15 Nov 1988).
- Rogalski, A. and K. Chrzanowski. "Infrared Devices and Techniques." *Opto-Electronics Review*. Vol. 10, No. 2: 111-136. (2002).
- Rork, Eugene W., and others. "Ground-Based Electro-Optical Surveillance of Satellites in Daylight by Detection of Reflected Sunlight," *EASCON '83: 16th Annual IEEE Electronics and Aerospace Systems Conference and Exposition Proceedings*: 103-109 (1983).

Singer, Jeremy. "Surveillance is Pressing Space Control Need." *C4ISR: The Journal of Net-Centric Warfare*. 22 October 2004.

Space Environment Technologies. *SOLAR2000*.
<http://www.spacewx.com/solar2000.html>. (2005).

Stroble, Nick. "Nick Stroble's Astronomy Notes."
<http://www.astronomynotes.com/nakedeye/s6.htm>. (2004). Accessed 16 Feb 06.

Wolfe, W. L., and G. J. Zissis, Ed., *The Infrared Handbook*, 3rd Ed. Washington, D.C.: The Infrared Information Analysis Center, Environmental Research Institute of Michigan, for the Office of Naval Research, Department of the Navy, 1989.

| REPORT DOCUMENTATION PAGE | | | | Form Approved OMB No. 074-0188 | |
|--|---------------|-----------------------------------|---|---|---|
| <p>The public reporting burden for this collection of information is estimated to average 1 hour per response, including the time for reviewing instructions, searching existing data sources, gathering and maintaining the data needed, and completing and reviewing the collection of information. Send comments regarding this burden estimate or any other aspect of the collection of information, including suggestions for reducing this burden to Department of Defense, Washington Headquarters Services, Directorate for Information Operations and Reports (0704-0188), 1215 Jefferson Davis Highway, Suite 1204, Arlington, VA 22202-4302. Respondents should be aware that notwithstanding any other provision of law, no person shall be subject to a penalty for failing to comply with a collection of information if it does not display a currently valid OMB control number.</p> <p>PLEASE DO NOT RETURN YOUR FORM TO THE ABOVE ADDRESS.</p> | | | | | |
| 1. REPORT DATE (DD-MM-YYYY) 22-03-2006 | | 2. REPORT TYPE Master's Thesis | | 3. DATES COVERED (From – To) Sep 2004 – Mar 2006 | |
| 4. TITLE AND SUBTITLE Radiometric Analysis of Daytime Satellite Detection | | | | 5a. CONTRACT NUMBER | |
| | | | | 5b. GRANT NUMBER | |
| | | | | 5c. PROGRAM ELEMENT NUMBER | |
| 6. AUTHOR(S) Lilevjen, Katherine, B., 2 nd Lieutenant, USAF | | | | 5d. PROJECT NUMBER | |
| | | | | 5e. TASK NUMBER | |
| | | | | 5f. WORK UNIT NUMBER | |
| 7. PERFORMING ORGANIZATION NAMES(S) AND ADDRESS(S) Air Force Institute of Technology Graduate School of Engineering and Management (AFIT/EN) 2950 Hobson Way WPAFB OH 45433-7765 | | | | 8. PERFORMING ORGANIZATION REPORT NUMBER AFIT/GAP/ENP/06-09 | |
| 9. SPONSORING/MONITORING AGENCY NAME(S) AND ADDRESS(ES) AFRL/SNJW Attn: Mark G. Nosek 2241 Avionics Circle Suite 2 WPAFB OH 45433-7304 (927) 255-4174 ext. 4020 | | | | 10. SPONSOR/MONITOR'S ACRONYM(S) | |
| | | | | 11. SPONSOR/MONITOR'S REPORT NUMBER(S) | |
| 12. DISTRIBUTION/AVAILABILITY STATEMENT APPROVED FOR PUBLIC RELEASE; DISTRIBUTION UNLIMITED. | | | | | |
| 13. SUPPLEMENTARY NOTES | | | | | |
| 14. ABSTRACT <p>A radiometric model for daylight satellite detection is developed and used to evaluate the effects of various parameters on signal-to-noise ratio (SNR). Detection of reflected sunlight from a low-earth orbit, diffuse, planar satellite by a single-pixel infrared photovoltaic detector is considered. Noise considered includes photon noise from the background and signal, as well as thermal noise. Parameters considered include atmospheric conditions, optical parameters, and detector parameters. The Phillips Laboratory Expert-assisted User System, an atmospheric modeling tool that employs the MODTRAN and FASCODE transmission codes, is used to model wavelength-dependent atmospheric transmission and background radiance.</p> <p>The SNR is found to increase when the detector is placed at higher altitudes and when there is lower aerosol content in the atmosphere. The SNR is also found to increase with decreased noise-equivalent bandwidth, detector dark current and field of view (FOV), and with larger optical elements. For a 16" diameter telescope and a FOV no smaller than 70 mrad, optimal bands are found to be between 0.8 µm and 1.7 µm.</p> | | | | | |
| 15. SUBJECT TERMS Daytime Satellite Detection, Daylight Satellite Detection, Artificial Satellites, Optical Detection, Signal to Noise Ratio, Radiometry, Satellite Tracking Systems | | | | | |
| 16. SECURITY CLASSIFICATION OF: | | | 17. LIMITATION OF ABSTRACT UU | 18. NUMBER OF PAGES 93 | 19a. NAME OF RESPONSIBLE PERSON Michael A. Marciniak, (ENP) |
| REPORT U | ABSTRACT U | c. THIS PAGE U | | | 19b. TELEPHONE NUMBER (Include area code) (937) 255-3636, ext 4529; e-mail: Michael.Marciniak@afit.edu |

Standard Form 298 (Rev. 8-98)
Prescribed by ANSI Std. Z39-18